

1 **Evaporite thickness and composition influence rift structural style,**
2 **Zechstein Supergroup, offshore Norway**

3
4 Christopher A-L. Jackson^{1*}, Gavin M. Elliott^{1‡}, Elisabeth Royce-Rogers^{1‡},
5 Rob L. Gawthorpe², Tor E. Aas³

6
7 ⁽¹⁾ *Basins Research Group (BRG), Department of Earth Science and Engineering, Imperial College,*
8 *Prince Consort Road, London, SW7 2BP, UK*

9
10 ⁽²⁾ *Department of Earth Science, University of Bergen, Allegate 41, N-5007 Bergen, Norway*

11
12 ⁽³⁾ *Statoil ASA, 4313 Sandnes, Norway*

13
14 ^(‡) *Now at: TGS, 1 The Crescent, Surbiton, Surrey, KT6 4BN, UK*

15
16 ^(*) *Now at: Lukoil Overseas UK Ltd, 5-11 Regents Street, London, SW1Y 4LR, UK*

17
18 *Corresponding author (e-mail: c.jackson@imperial.ac.uk)

19
20 **ABSTRACT**

21
22 ‘Salt’ giants are typically halite-dominated, although syn-depositional variations in water depth, and
23 fluctuations in climate and basin hydrology, result in interlaying of other evaporite (e.g. anhydrite, bittern
24 salts) and non-evaporite (e.g. carbonates, clastics) rocks. These rocks have different mechanical
25 properties, thus they impact or respond to rift-related crustal deformation in different ways. However, our
26 understanding of how lithology varies at the basin-scale in ancient salt giants, what controls this, or how
27 these variations impact later rift-related deformation, is poor, principally due to a lack of seismic
28 reflection-borehole datasets that are of sufficient regional extent. Here we use regional 2D seismic
29 reflection and borehole data from offshore Norway to map compositional variations within the Zechstein
30 Supergroup (Upper Permian), one of the world’s best known salt giants. Regional stratigraphic panels
31 illustrate the vertical and lateral variability of evaporite and non-evaporite rocks in the Zechstein
32 Supergroup; 2D seismic reflection data allow us to relate compositional variations to basin structure and,
33 in particular, Middle Jurassic-to-Early Cretaceous rift-related structural styles. We show that the

34 Zechstein Supergroup is dominated by mainly halite, anhydrite and carbonate, with minor amounts of
35 claystone, sandstone and potassium salts. Based on the proportion of halite, we identify and map four
36 intrasalt DZs (*sensu* Clark et al., 1998) across the Norwegian sector of the North Sea Basin. We show
37 that, at the basin margins, the Zechstein Supergroup is carbonate-dominated, whereas towards the basin
38 centre, it become increasingly halite-dominated, a trend observed in the UK sector of the North Sea Basin
39 and in other ancient salt giants. However, we also document abrupt, large magnitude compositional and
40 thickness variations adjacent to large, intra-basin normal faults; for example, thin, carbonate-dominated
41 successions occur on fault-bounded footwall highs, whereas thick, halite-dominated successions occur
42 only a few kilometres away in adjacent depocentres. It is presently unclear if this variability reflects
43 variations in syn-depositional relief related to flooding of an underfilled presalt (Early Permian) rift or
44 syn-depositional (Late Permian) rift-related faulting. Irrespective of the underlying controls, variations in
45 salt composition and thickness influenced the Middle Jurassic-to-Early Cretaceous rift structural style,
46 with diapirism characterising hangingwall basins where autochthonous salt was thick and halite-rich, and
47 salt-detached normal faulting occurring on the basin margins and on intra-basin structural highs where the
48 salt was too thin and/or halite-poor to undergo diapirism. This variability is currently not captured by
49 existing tectono-stratigraphic models largely based on observations from salt-free rifts and, we argue,
50 mapping of suprasalt structural styles may provide insights into salt composition and thickness in areas
51 where boreholes are lacking or seismic imaging is poor.

52

53 INTRODUCTION

54

55 The term ‘salt’ is typically used to describe halite-dominated rocks. However, ‘salt’ sequences may
56 contain other evaporite rocks such as anhydrite or, its hydrated form, gypsum, and non-evaporite rocks
57 such as carbonates and clastics (e.g. Warren, 1999; Hudec and Jackson, 2007). These rocks have different
58 mechanical properties and will accordingly show different styles of deformation when stressed (i.e.
59 faulting of carbonates and clastics, flow of halite). These variations in lithology and mechanical property,
60 in addition to the bulk thickness of the salt and its overburden, are important to consider when examining
61 the structural evolution of rifts forming crust that contains thick salt sequences. For example, the
62 structural style and evolution of rifts containing relatively thick salt (e.g., Stewart et al., 1996, 1997;
63 Pascoe et al., 1999; Withjack and Callaway, 2000; Richardson et al., 2005; Stewart 2007; Kane et al.,
64 2010; Wilson et al., 2013) differ significantly from salt-free rifts (Leeder and Gawthorpe, 1987; Prosser,
65 1993; Gawthorpe and Leeder, 2000). These differences arise because salt influences the degree and style
66 of coupling between sub- and suprasalt deformation, and because activity on sub- and suprasalt faults can

67 trigger salt flow and halokinesis. As a result, the physiography of and sediment dispersal patterns in, salt-
68 influenced rifts may be more complex than in salt-free rifts, thus questioning the general applicability of
69 widely used rift tectono-stratigraphic models (Gawthorpe and Leeder, 2000).

70 The Zechstein Supergroup is one of the world's best-known and largest salt giants, documenting
71 repeated flooding and evaporation of a continent-scale saline water body that covered much of the NW
72 Europe during the Late Permian. Notably, the Zechstein Supergroup occurs within the prerift succession
73 to and likely influenced the development of, the Middle Jurassic-to-Early Cretaceous rift. To-date, most
74 studies of Zechstein Supergroup compositional variations have focussed on the southern North Sea and
75 the north-western margin of the North Permian Basin (Fig. 1). For example, Clark et al. (1998), using
76 seismic reflection and very sparse borehole data from the north-western margin of the North Permian
77 Basin, demonstrate the Zechstein Supergroup is characterised by a thick sequence of halite and anhydrite
78 in the basin centre, and a relatively thin carbonate-clastic sequence at the basin margin (Figs 2 and 3).
79 Based on the overall thickness and seismic expression of the Zechstein Supergroup, and the approximate
80 percentage of halite, Clark et al. (1998) map four basin-scale DZs (DZ1-4; see also Taylor, 1990). DZ1,
81 which contains <10% halite, occurs at the basin margin or on normal fault-bound, intra-basin structural
82 highs (Fig. 3). DZ2 (10-50% halite) and DZ3 (50-80% halite) occur on basinward-dipping ramp-like
83 areas, whereas DZ4 (>80 % halite), which constitutes the majority of the fill of the North Permian Basin,
84 occurs towards the basin centre (Fig. 3). It should be noted that, although elegant, the model of Clark et
85 al. (1998) is supported by only sparse borehole data

86 Compared to the UK sector, almost nothing is known about basin-scale compositional variations
87 in the Zechstein Supergroup in the Norwegian sector of the North Sea Basin. Jackson and Lewis (2016)
88 recently used 3D seismic and reflection data from the Sele High Fault System, eastern Sele High to
89 document rapid across-fault variations in salt thickness and composition, demonstrating that the footwall
90 apex of this large displacement (>2 km) is capped by relatively thin (58 m), largely immobile carbonate
91 and claystone, whereas relatively thick (>200 m), mobile halite occurs in the adjacent hangingwall.
92 Although insightful, the study of Jackson and Lewis (2016) covers only a relatively small area (c. 3600
93 km²) and, to-date, there has been no systematic regional study of basin-scale compositional variability in
94 the Zechstein Supergroup. Establishing this is important for two key reasons. First, given that they appear
95 directly related to syn-depositional basin structure, compositional variations may shed light on the Late
96 Permian physiography of the Norwegian sector of the North Permian Basin. More specifically, they may
97 reveal whether salt deposition occurred in a large unfaulted sag-like basin following an earlier period of
98 rifting, or in an active rift. Second, and because of variability in the mechanical properties of evaporite
99 and non-evaporite rocks, intra-Zechstein compositional variations may influence the structural style and

100 evolution of the Middle Jurassic-to-Early Cretaceous rift, which, at least in its southern reaches, developed
101 in the presence of salt.

102 We here use borehole data to map basin-scale (*c.* 30000 km²) variations in Zechstein Supergroup
103 composition on the north-eastern margin of the North Sea Basin. We also use long-offset, 2D seismic
104 reflection data to examine variations in Zechstein Supergroup thickness and geometry, and to constrain
105 the present sub- and suprasalt structure of the study area. By combining stratigraphic and structural data
106 we are able to investigate the role that composition variations in the Zechstein Supergroup had on the syn-
107 rift structural styles and evolution of the Middle Jurassic-to-Early Cretaceous rift system. We show that
108 compositional variations in the Zechstein Supergroup are strongly controlled by syn-depositional basin
109 relief; this relief may have been inherited from an earlier tectonic event, or have formed during salt
110 deposition. Furthermore, variations in salt composition and thickness strongly influenced the Middle
111 Jurassic-to-Early Cretaceous rift structural style, with classic salt-tectonic structural styles forming in
112 areas where the autochthonous salt was thick and halite-rich. Based on our findings, we suggest current
113 rift basin tectono-stratigraphic models need modifying to take into account the presence of pre-rift salt.

114

115 **TECTONO-STRATIGRAPHIC FRAMEWORK**

116

117 The study area is located in the Norwegian sector of the northern North Sea, with particular focus on the
118 South Viking Graben, Utsira High, Ling Graben and Egersund Basin (Fig. 1). Carboniferous-to-Early
119 Permian transtension drove initial normal fault-related basin subsidence and led to the formation of the
120 Egersund Basin, and the South Viking, Ling and Åsta grabens (Coward, 1995; Roberts *et al.*, 1995;
121 Glennie, 1998; Coward *et al.*, 2003; Zanella and Coward, 2003). Following continental extension, Late
122 Permian thermal subsidence resulted in formation of the pan-European, North Permian Basin, which was
123 subsequently overprinted by the Middle Jurassic-to-Early Cretaceous rift-related basins listed above (Fig.
124 1A). The study area lay towards the northern and north-western margins of the North Permian Basin (Fig.
125 1). A relative sea-level rise in the earliest Late Permian established marine-to-marginal marine conditions
126 in the North Permian Basin, and repeated cycles of basin flooding and desiccation drove deposition of a
127 >1 km thick, evaporite-dominated unit (Zechstein Supergroup, herein referred to as ‘salt’; Figs 1 and 2).
128 Previous studies suggest that the Zechstein Supergroup was up to 1.5 km thick in the South Viking
129 Graben and Egersund Basin, and indicate that carbonates and clastics at the basin margins pass
130 basinwards into anhydrites and halites in the basin axes (Pegrum and Ljones 1984; Sørensen *et al.*, 1992;
131 Thomas and Coward 1996; Evans *et al.*, 2003; Jackson *et al.* 2010; Jackson & Lewis, 2016).

132 The abundance of salt structures (e.g. pillows, diapirs) and rapid, large-magnitude variations in
133 the thickness of Triassic deposits confirms that post-depositional flow of Zechstein Supergroup salt
134 occurred in the South Viking and Ling grabens during the Triassic (Pegrum and Ljones, 1984; Sørensen
135 et al., 1992; Erratt, 1993; Thomas and Coward, 1996, Jackson and Larsen, 2009; Kane *et al.*, 2010). In
136 contrast, the Åsta Graben, which likely contained thinner and/or less mobile evaporites, was less affected
137 by salt movement and was instead dominated by rift-related extension and faulting. In the Early Jurassic,
138 impingement of a mantle plume at the base of the lithosphere led to the formation of the Mid-North Sea
139 Dome, which drove transient uplift of much of the southern Viking Graben, the Moray Firth, and the
140 north and north-east Central Graben. Because of this major tectonic event, Triassic and older stratigraphic
141 units were locally completely eroded and Early Jurassic strata are locally absent due to non-deposition or
142 erosion. During the Middle to Late Jurassic, a combination of the collapse of the Mid-North Sea Dome
143 and extensional faulting led to flooding of the North Sea Rift System (Cockings *et al.*, 1992; Thomas and
144 Coward, 1996; Coward *et al.*, 2003; Lyngsie *et al.*, 2006).

145 Crustal extension during the Late Jurassic and Early Cretaceous reactivated many of the Permo-
146 Triassic, basement-involved normal fault system bounding the main structural elements (e.g. the Graben
147 Bounding Fault Zone that bounds the western margin of the South Viking Graben; the Sele High and
148 Stavanger fault systems that bound the Egersund Basin and Åsta Graben; Lewis et al., 2013; Jackson &
149 Lewis, 2016). Basement-involved faulting and tilting during the Late Jurassic and Early Cretaceous also
150 drove salt flow and the growth of diapirs, extension of supra-salt strata, and formation of salt-detached
151 (supra-salt) normal fault arrays (Thomas and Coward, 1996; Jackson and Larsen, 2009; Lewis et al.,
152 2013; Tvedt et al., 2013; Jackson and Lewis, 2016). This study focuses on: (i) basin-scale variations in
153 Zechstein Supergroup thickness and composition in the Norwegian sector of the North Sea (cf. Stewart,
154 2007); and (ii) the hitherto undocumented role that Zechstein Supergroup thickness and compositional
155 variations played in controlling basin-scale variations in the structural style of the Late Jurassic-to-Early
156 Cretaceous rift event.

157 Although some of the larger structures continued to be active, many of the rift-related normal
158 faults became inactive during the Early Cretaceous in response to declining rates of crustal extension
159 (Knott *et al.*, 1993; Thomas and Coward, 1996; Knott, 2001; Fraser *et al.*, 2003). During the Late
160 Cretaceous to Cenozoic, the Northern North Sea subsided due to cooling of the crust following Late
161 Jurassic-to-Early Cretaceous rifting; subsidence was, however, punctuated by a period of inversion that
162 resulted in squeezing and amplification of salt diapirs and local reverse reactivation of normal faults (e.g.
163 Biddle and Rudolph, 1988; Cartwright, 1989; Sørensen et al., 1992; Fraser et al 2003; Jackson et al.,
164 2013).

165

166 **DATASET AND METHODS**

167

168 This study integrates wireline log data from 22 wells and 2D seismic reflection profiles covering
169 Norwegian North Sea exploration blocks 8-10, 16-18 and 25 (Fig. 1). The seismic profiles are spaced
170 every c. 5 km in the south-east and c. 10 km in the north-west of the study area. The seismic data are
171 time-migrated and are presented in two-way time (TWT). The record length is 9 sec TWT, which is
172 sufficient for imaging subsalt units across much of the basin. All profiles are displayed with ‘normal’
173 polarity (i.e. an increase in acoustic impedance with depth is represented by peak or black reflection,
174 whereas a decrease in acoustic impedance with depth is represented by trough or red reflection; see
175 Brown, 2004). Twenty-two exploration wells, which fully or partially penetrate the Zechstein Supergroup,
176 allow a petrophysical characterisation of the key lithologies within the Zechstein Supergroup and regional
177 and local mapping of these units (Fig. 1 and Table 1). Key lithostratigraphic or chronostratigraphic
178 surfaces were identified in wells and tied to the seismic data. Five regionally correlatable seismic horizons
179 were interpreted: (i) top Rotliegend Group (top Lower Permian); (ii) top Zechstein Supergroup (top Upper
180 Permian); (iii) top Smith Bank Formation (approximate top Triassic); (iv) Base Cretaceous Unconformity
181 (BCU) (top Jurassic); and (v) top Shetland Group (Base Palaeogene Unconformity or BPU) (Fig. 2).
182 Based on the distribution of seismic and well data we define two main study areas; a northern area that
183 focuses on the South Viking Graben, Utsira High and Sleipner Terrace, and a southern area focused on
184 the Ling Graben, Sele High and Egersund Basin (Fig. 1).

185 To identify evaporite and non-evaporite lithologies in the Zechstein Supergroup we combined
186 observations from wireline petrophysical logs and cuttings data (from well reports and composite logs)
187 from 10 of the 22 wells. Cuttings data were used to identify the principal Zechstein Supergroup
188 lithologies, whose petrophysical expression was then constrained by extracting corresponding log values
189 at 1, 10 and 20 m intervals, depending on unit thickness (i.e. 0-500 m, 500-1000 m and >1000 m thick
190 respectively). A total of 1307 points were extracted and used to create cross-plots (i.e. Sonic vs. Density;
191 GR vs. Sonic); these cross-plots defined petrophysical ranges for each lithology that then allowed us to
192 interpret lithology variations from wireline logs in wells (or sections of wells) lacking cuttings data (see
193 next section). We then defined seven lithologies or ‘petrophysical facies’: (i) anhydrite; (ii) halite; (iii)
194 carnallite (i.e. a hydrated, potassium chloride evaporite); (iv) ‘carbonate’ (dolomite and limestone); (v)
195 shale-claystone; (vi) siltstone, and (vii) sandstone (Fig. 4 and Table 2).

196 Regional stratigraphic correlations based on well data and tied to regional seismic reflection
197 profiles were then constructed to examine the lateral variation in Zechstein Supergroup lithology and

198 thickness. These combined well log/seismic stratigraphic correlations allowed the structural context of
199 individual wells to be identified (i.e. whether a well is located in the basin centre, at the basin margin, on
200 an intra-basin structural high, in a major salt structure, etc). However, due to a lack of biostratigraphic
201 data and because of substantial post-depositional salt flow, it is not possible to correlate individual, metre-
202 to decametre-scale, evaporite or non-evaporite stratigraphic packages within the Zechstein Supergroup.
203 We also note that post-depositional flow of salt led to the growth of diapirs, which, despite being
204 relatively small compared to those observed elsewhere in the northern North Sea (e.g. Davison et al.,
205 2000; Stewart, 2007), likely disrupted the primary (i.e. depositional) lithology distribution within the
206 Zechstein Supergroup. However, the seismic reflection and borehole data we present below suggest the
207 latter still provide a fair record of the primary lithology distribution; more specifically, areas dominated
208 by thick, halite-dominated sequences are characterised by diapiric structures, whereas those characterised
209 by thin, halite-poor sequences lack such structures.

210

211 **PETROPHYSICAL EXPRESSION OF THE ZECHSTEIN SUPERGROUP**

212

213 Density (RHOB)-Sonic (DT) cross-plots were used to differentiate between halite and anhydrite; halite
214 has relatively low RHOB values (2-2.3 g/cm³) and moderate DT values (>65 μs/ft), whereas anhydrite has
215 moderate RHOB values (typically >2.7 g/cm³) and low DT values (typically <65 μs/ft) (Fig. 4). Overlap
216 of the anhydrite and carbonate fields on RHOB-DT cross-plots suggests the anhydrite may be impure (see
217 below) (Fig. 4). Carbonate and claystone are characterised by a very wide range of RHOB (1.9-3.1 g/cm³)
218 and DT (50-90 μs/ft) values making it impossible to discriminate between these in wells lacking cuttings.
219 Cross-plotting of GR vs. RHOB and GR vs. DT data also indicate it is difficult to differentiate between
220 carbonate and claystone (Fig 5). The highly variable and overlapping petrophysical characteristics of
221 these lithologies suggest: (i) they were incorrectly identified in cuttings data; or (ii) they are impure,
222 containing an admixture of, for example, anhydrite and shale-claystone (i.e. a ‘dirty’ anhydrite). Despite
223 the limitations of our wireline log-based analysis, we feel it provides a good first-order assessment of
224 lithology variations in the Zechstein Supergroup.

225

226 **DISTRIBUTION, THICKNESS AND LITHOLOGY OF ZECHSTEIN SUPERGROUP SALT**

227

228 A regional two-way time (TWT) thickness map shows that the Zechstein Supergroup is typically c. 200
229 ms thick, but is up to 1000 ms thick in diapirs located in the axes of the major fault-bound depocentres
230 (e.g. the Ling Graben, where diapirs are penetrated by 16/11-1S and 16/8-2; Fig. 6; see also seismic

231 profiles in Figs. 7-10). Towards the eastern margin of the South Viking Graben the Zechstein Supergroup
232 is relatively thin (<100 ms TWT) and salt structures are sparse. The Zechstein Supergroup is also thin on
233 intra-basin structural highs such as Sele High (<60 m; 17/12-2) and Sleipner Terrace (<100 m; 16/1-2).
234 Seismic data thus suggest a first-order positive relationship between the present thickness and mobility of
235 the Zechstein Supergroup (e.g. thick Zechstein Supergroup is mobile; thin Zechstein Supergroup is
236 immobile; Jackson & Lewis, 2016). Furthermore, basement-involved normal faults appear to exert a
237 primary control on the Zechstein Supergroup thickness, with the unit being thinnest on basin margin or
238 intra-basin, fault-bound structural highs (e.g. Sele High and flanks of Utsira High), and thickest in deep
239 basins such as the Ling Graben (Fig. 6). Below we describe the thickness and composition in the
240 Zechstein Supergroup in three sub-areas, relating this to the styles of salt- and rift-related deformation.

241

242 **Study Area 1: South Viking Graben, Sleipner Terrace and Utsira High**

243

244 The correlation panel in Figure 7 illustrates variations in thickness and lithology of the Zechstein
245 Supergroup between relatively deep depocentres such as the South Viking and Ling grabens, and
246 relatively shallow, basin margin locations such as the western margin of the Utsira High and the Sleipner
247 Terrace. Four wells (15/5-3, 16/4-1, 15/9-9 & 15/12-3) on this panel penetrate the entire Zechstein
248 Supergroup succession, whereas 15/12-2 only penetrates its upper 37 m. Wells located in the axis of the
249 South Viking Graben (15/5-3) and Ling Graben (15/12-3) penetrate diapirs and indicate that the Zechstein
250 Supergroup, which in well 15/5-3 is up to 1046 m thick, is dominated by halite (93% of the penetrated
251 thickness) with relatively thin (<30 m) intervals of anhydrite and more rarely, carnallite. Using the
252 scheme of Clark et al. (1998), 15/5-3 lies in DZ4. In the axis of the Ling Graben the Zechstein
253 Supergroup is 1203 m thick, with the upper 743 m being halite-dominated and containing thin (<5 m)
254 carnallite layers (15/12-3; Fig. 7A). The lower 260 m of the succession is claystone-dominated, with
255 relatively thin (<30 m) anhydrite and halite intervals. Overall, 15/12-3 comprises >70% halite and it
256 therefore lies within DZ3. Seismic data indicate that, in these deep basin locations, where the Zechstein
257 Supergroup is relatively thick and halite-dominated (i.e. DZ3-4), large diapirs (Figs 7B and 8B). Thinning
258 and onlap of the Triassic succession across these salt structures suggests salt flow occurred during the
259 Triassic; a later period of flow during the Middle to early Late Jurassic is also locally indicated by
260 thinning and onlap of the corresponding interval across some of the salt-cored structures (Fig. 7).

261 In contrast to the deep basin wells, 16/4-1 and 15/9-9, which are located on present-day structural
262 highs situated at the basin margins, contain a relatively thin, halite-poor Zechstein Supergroup (Fig. 7). In
263 16/4-1, located on the western margin of the Utsira High, the Zechstein Supergroup is dominated by

264 clastic lithologies (siltstone and sandstone) with only minor anhydrite and carbonate. Likewise, 15/9-9,
265 located on the Sleipner Terrace, is largely composed of anhydrite with minor carbonate; halite is lacking.
266 The halite-poor nature of these wells places both of these wells and the domains they represent within
267 DZ1. Seismic data indicate that at the basin margins, where the Zechstein Supergroup is relatively thin
268 and halite-poor (i.e. DZ1), salt structures are very rare, with very little relief being developed at top salt
269 (Fig. 7B).

270 A correlation panel along the western flank of the Utsira High further illustrates the variations in
271 thickness and lithology occurring in the Zechstein Supergroup at the basin margin (Fig. 9). Four wells
272 completely penetrate a relatively thin (<150 m) Zechstein Supergroup succession, but only 16/1-2 and
273 16/7-2 occur close to seismic reflection profiles (Fig. 9). All of the wells lack halite and are dominated by
274 non-evaporitic lithologies such as carbonate, fine-grained clastics and anhydrite. In the most northern
275 well, evaporite facies are completely absent and the Zechstein Supergroup is composed only of claystone
276 and carbonate (25/10-4R). Well 25/10-2R, which is located on the western flank of the Utsira High, is
277 carbonate-rich (50%), particularly towards its base, but it also contains anhydrite with a thin shale-
278 claystone layer at the top of the Zechstein Supergroup. Well 16/1-2, is also carbonate-dominated,
279 although anhydrite occurs in the middle of the Zechstein Supergroup and claystone is found towards its
280 top and base (Fig. 9). The upper and lower parts of the Zechstein Supergroup in well 16/7-2, located at the
281 southern tip of the Utsira High, are carbonate-rich, although anhydrite and shale-claystone are prevalent
282 in the middle part of the well. Based on their lack of halite, wells along the flanks of the Utsira High are
283 representative of DZ1. As we observed for the south-western Utsira High and the Sleipner Terrace, salt
284 structures are absent on the basin margins where the Zechstein Supergroup is relatively thin and halite-
285 poor (i.e. DZ1). Furthermore, basement-involved faults cross-cut the Zechstein Supergroup ‘salt’ and
286 extend up into the Mesozoic succession (Fig. 9B).

287

288 **Study Area 2: Ling Graben, Sele High and Åsta Graben**

289

290 Two broadly E-trending correlation panels illustrate the variations in Zechstein Supergroup thickness and
291 lithology occurring between the present basin margins (i.e. Sleipner Terrace) and intra-basin highs (i.e.
292 Sele High; Fig. 8), and the adjacent fault-bound depocentres (i.e. Ling and Åsta grabens; Fig. 10).
293 Beginning with the most northerly of these two panels (Fig. 8), our data show that, on the Sleipner
294 Terrace, the Zechstein Supergroup is 25–64 m thick and it is notable for its lack of halite. Instead, the
295 Zechstein Supergroup is dominated by anhydrite (74%; 15/9-16) or claystone (48%; 16/7-3), with
296 moderate amounts of carbonate (26-27% in 15/9-16 and 16/7-3). The Zechstein Supergroup succession is

297 thus compositionally similar to that encountered along the eastern flank of the South Viking Graben, on
298 the margin of the Utsira High (cf. Fig. 9). 16/8-2 and 16/9-1, which are located within the Ling Graben
299 only 17 km to the east of 16/7-3, are separated from the Sleipner Terrace by a south-eastward dipping,
300 NE-SW-striking normal fault that has 660 ms of throw at top Lower Permian (top Rotliegend) level (Figs.
301 1 and 8B). In the hangingwall of the fault, 16/8-2 penetrated a salt wall at least 1325 m thick and
302 comprising 94% halite with minor amounts of anhydrite, carbonate and carnallite; the Zechstein
303 Supergroup in this location can be placed in DZ4. Well 16/9-1, which is also located on the western flank
304 of the Sele High, only penetrated the upper 140 m of a c. 350 m thick Zechstein Supergroup succession,
305 with the penetrated interval dominated by anhydrite (63%), although halite is present (35%), together with
306 a thin (<10 m) claystone unit cap (Fig. 8). Based exclusively on the lithologies encountered in its upper
307 part, the Zechstein Supergroup is assigned to DZ3. Seismic data indicate again that structural style is
308 closely coupled to Zechstein Supergroup thickness and composition; on the basin margins, where the unit
309 is thin and halite-poor (i.e. DZ1-2), no salt structures or only very low-relief pillows occur, with normal
310 faults cross-cutting the salt and extending from subsalt into suprasalt strata (i.e. Sele High and Sleipner
311 Terrace; Fig. 8B). In contrast, in the basin centre, where the unit is thick and halite-rich (i.e. DZ3-4),
312 diapirs are common (i.e. Ling Graben; Fig. 8B). Salt-detached normal faults, which extend up into
313 Tertiary strata, are also developed in basin centre locations (Fig. 8B).

314 The southerly of the two panels further highlights the lateral lithology and thickness variations
315 occurring in the Zechstein Supergroup between intra-basin, fault-bound highs and adjacent depocentres
316 (Fig. 10). 16/10-1, 16/11-1S and 17/11-1 are located within the Ling Graben and, although none of these
317 wells penetrate the entire thickness of the Zechstein Supergroup, through the use seismic data it is
318 possible to constrain the approximate thickness of the Zechstein Supergroup at each well location by
319 projecting the wells onto the seismic data. This exercise suggests 16/10-1 penetrates the upper 35 m of a
320 salt wall that is c. 315 m thick (Fig. 10A). Wireline-log data suggest the Zechstein Supergroup is
321 dominated by halite (66%), with anhydrite, claystone and rare carnallite occurring in the upper few tens of
322 metres (DZ3). 16/11-1S also penetrates a salt wall and seismic data indicate the Zechstein Supergroup in
323 this location is c. 820 m thick (Fig. 10). The upper 794 m of the Zechstein Supergroup is penetrated in
324 this well, with wireline-log data indicating it is composed almost entirely of halite (99%) with minor
325 amounts of anhydrite and carbonate in the upper 38 m (DZ4). 17/11-1 in the Ling Graben penetrates the
326 Zechstein Supergroup in an area that appears to have undergone relatively limited amounts of post-
327 depositional salt flow. The well penetrates a 755 m thick succession of the Zechstein Supergroup, with
328 seismic data suggesting a further c. 15 m of Zechstein Supergroup occurs beneath the base of the well. In
329 this location the Zechstein Supergroup is dominated by halite (78%), with carnallite and carbonate-rich

330 intervals occurring in the lower 50 m, and anhydrite and carbonate-rich intervals occurring in the upper
331 20 m (Fig. 10). Decimetre-thick carbonate intervals also occur in the upper third of the unit. Based on
332 these bulk lithological variations, the Zechstein Supergroup in this location is assigned to DZ3. 17/12-2,
333 which is located 22 km updip to the east of 17/11-1, on the eastern margin of the Sele High, in the
334 immediate footwall of the Sele High Fault System, fully penetrates a thin (49 m), carbonate-dominated
335 (84%) Zechstein Supergroup (DZ1). 17/12-1R, which is located 15 km to the east of 17/12-2 and in the
336 hangingwall of the Sele High Fault System, penetrates the upper 160 m of a c. 250 m thick salt pillow
337 (Fig. 10B). The Zechstein Supergroup in the well is composed predominantly of halite (69%), although
338 the upper 27 m is dominated by anhydrite and claystone, placing it within DZ3. The area covered by Fig.
339 10 shows the same relationship between basin structural style and Zechstein Supergroup thickness and
340 composition as observed elsewhere.

341 When considering the salt- and rift-related structural styles we note that large Triassic-to-Jurassic
342 minibasins are flanked by diapirs in the basin centre and on the lower flanks of intra-basin highs where
343 the Zechstein Supergroup is thick and halite-rich (i.e. DZ3-4) (i.e. Ling Graben; Fig. 10B). On crests of
344 intra-basin fault-bound highs, where the unit is thin and halite-poor (i.e. DZ1-2), no large salt structures
345 occur, although small rollers are present in the footwalls of salt-detached faults (i.e. Sele High; Fig. 10B).
346 However, downdip of structural culminations such as the Sele High, in an areas ascribed to DZ3 (i.e. 50-
347 80% halite), seismic data image a range of salt-related structures including diapirs, minibasins and rafts
348 (Figs 11, 12, and 13).

349

350 **Study Area 3: Egersund Basin and Lista Nose**

351

352 A correlation panel (Fig. 4) covering the south-eastern part of the Egersund Basin and the north-eastern
353 edge of the Lista Nose illustrates lithological variations in the Zechstein Supergroup immediately adjacent
354 to the Stavanger Platform. Based on the lithology of the Zechstein Supergroup sampled by wells in this
355 location, the Zechstein Supergroup has been assigned to DZ1 (i.e. 10/7-1 and 10/5-1) and 3 (i.e. 10/8-1).
356 For example, 10/7-1, located on the eastern edge of the Egersund Basin, appears to sample the upper 45 m
357 of a diapir flank. The well lacks halite and is composed solely of non-evaporitic lithologies; the lower part
358 of the well is clastic-dominated whereas the upper part of the well is dominated by carbonate (Fig. 4).
359 Again, because 10/7-1 well only penetrates the upper part of the salt, assigning a depositional zone is not
360 straightforward. Strictly speaking, the well lies in the footwall of a major normal fault in an area of thin
361 salt; however, it penetrates a diapir that at least partly overlies the adjacent footwall. As such, we infer
362 that well straddles the boundary between an area of thick, mobile salt to the SW in the Egersund Basin

363 and thin, relatively immobile salt to the NE on the Lista Fault Blocks. In this context, the diapir was likely
364 fed by salt expelled from the hangingwall during rifting (cf. Burliga et al., 2012). 10/8-1, which is situated
365 on the Lista Nose, penetrates the core of a salt pillow and indicates the Zechstein Supergroup is composed
366 of anhydrite (12%) and claystone (22%) that overlie a halite-rich (66%) succession (DZ3). Finally, in
367 10/5-1, which is located near the boundary between the Lista Nose and the Stavanger Platform (Fig. 1),
368 the Zechstein Supergroup is 217 m thick and lacks halite. Instead, a 138 m thick, carbonate-rich
369 succession overlies an anhydrite and marl-rich unit that is underlain by a clastic-rich unit defining the
370 base of the Zechstein Supergroup (DZ1).

371

372 **RELATIONSHIP OF ZECHSTEIN SUPERGROUP THICKNESS AND COMPOSITION TO** 373 **SUBSALT BASIN STRUCTURE**

374

375 The present distribution of and lithological variations in the northern North Sea are summarised in Figure
376 15; this incorporates data presented here from the north-eastern margin of the North Permian Basin (i.e.
377 Norwegian sector of the northern North Sea), and data from the north-western and western margin of the
378 North Permian Basin (i.e. UK sector of the northern North Sea) presented by Clark *et al.* (1998), Glennie
379 et al. (2003), Stewart (2007) and Jackson et al. (2010) (see Fig. 3). In the Norwegian sector of the
380 northern North Sea, halite-poor successions (i.e. DZ1) occur towards the basin margins (e.g. western
381 margin of the Utsira High and the south-western margin of the Stavanger Platform). The Zechstein
382 Supergroup is also halite-poor on normal-fault bound, intra-basin structural highs (e.g. Sele High). Halite-
383 rich successions (i.e. DZ4) characterise relatively deep, basin centre locations (e.g. Ling Graben,
384 Egersund Basin and the axis of the South Viking Graben). Moderately halite-rich parts of the Zechstein
385 Supergroup (DZ2 and 3) occur in transitional areas, such as fault-bound, basin-margin terraces or on
386 largely unfaulted, gently basinward-dipping ramps (e.g. western margin of the Utsira High).

387 Data from the Norwegian and UK sectors of the northern North Sea clearly indicate that the
388 lithology of the Zechstein Supergroup is directly related to its thickness. For example, where it is <200 m
389 thick, the Zechstein Supergroup is halite-poor, and dominated by anhydrite and non-evaporitic lithologies
390 such as claystone, carbonate and siltstone. In contrast, in areas where it is >200 m thick, the Zechstein
391 Supergroup it is dominated by halite, although thin units of anhydrite and non-evaporitic lithologies occur
392 (cf. Figs 6 and 15). Relatively abrupt changes in lithology occur across basement-involved normal faults,
393 such as that observed between the Sleipner Terrace and the Ling Graben (Fig. 8), and between the Sele
394 High and the Egersund Basin (Figs 7 and 15). We note that not all lithological transitions are abrupt. For
395 example, between the South Viking Graben (e.g. 15/5-3), which is inferred to be halite-rich, and the

396 Utsira High (16/4-1), which is characterised by a halite-poor succession, no significant basement relief is
397 observed on seismic reflection profiles, implying that the variations in lithology between these locations
398 is gradational. A similar gradational lithology transition, which again appears unrelated to significant
399 basement relief, is evident between the Utsira High (e.g. 15/9-9) and Ling Graben (e.g. 15/12-3) (Figs 7
400 and 15).

401

402 **DISCUSSION**

403

404 **Controls on thickness patterns and lithological variations in salt giants**

405

406 Well and 2D seismic reflection data have allowed us to define the present thickness and lithological
407 variations in the Zechstein Supergroup along the northern margin of the North Permian Salt Basin. These
408 data indicate that the Zechstein Supergroup is thickest in the centre of the Late Jurassic basins, and thins
409 towards their margins and across fault-bound intra-basin structural highs; this relationship has previously
410 been inferred to reflect the syn-depositional extent and physiography of the North Permian Salt Basin
411 (Clark et al., 1998; Stewart, 2007; Jackson and Lewis, 2013). However, it is clear that, due to post-
412 depositional flow of the Zechstein Supergroup, the thickness and, potentially, the primary lithological
413 variability of the unit has been strongly modified and may not, therefore, reflect the syn-depositional
414 basin physiography. For example, does thinning of the Zechstein Supergroup onto the basement margins
415 reflect a primary depositional pinchout or merely an erosional boundary related to post-depositional
416 erosion/dissolution? Related to this, does the thin/halite-poor nature of the Zechstein Supergroup at the
417 basin margins and on intra-basin structural highs, and the thick/halite-rich nature of the unit of the unit in
418 the basin centre, reflect a eustatic control on deposition (see Tucker, 1991), or simply the impact of post-
419 depositional tectonics and erosion on preservation and composition?

420 We propose that one or a combination of the four following end-member models may account for
421 the thickness and lithology variations observed in the Zechstein Supergroup (Fig. 16; see also Jackson
422 and Lewis, 2013): (i) *Model 1* (Fig. 16a) - the Zechstein Supergroup was deposited within a largely
423 unstructured, bowl-shaped basin and was halite-rich across the entire basin, including the basin margins
424 and the future positions of intra-basin structural highs. Post-depositional uplift associated with subsequent
425 Triassic and/or Middle Jurassic-to-Early Cretaceous rifting resulted in erosion and dissolution of the
426 halite components of the Zechstein Supergroup, and the relative enrichment in non-halite lithologies at
427 the basin margins and on intra-basin structural highs. Erosion, dissolution and relative enrichment of the
428 Zechstein Supergroup in anhydrite may also have occurred in response to exposure of the Zechstein

429 Supergroup at the flexural rather than fault-bound basin margins of the North Permian Basin during
430 Triassic exposure; (ii) *Model 2* (Fig. 16b) – the Zechstein Supergroup was deposited in a largely
431 unstructured, bowl-shaped basin and was characterised by gradual changes in thickness and lithology,
432 with anhydrite-rich successions at the basin margin passing gradually basinwards into halite-rich
433 successions in the basin centre (Clark et al., 1998; Stewart, 2007). Post-depositional flow of the Zechstein
434 Supergroup was, however, strongly partitioned, with mobile halite being preferentially expelled from the
435 source layer on the basin margin into flanking salt structures, resulting in local enrichment of non-halite
436 lithologies in areas where the Zechstein Supergroup is thin. This model applies not only to areas where
437 salt is thin due to the subsalt basin structure, but also due to welding due to post-depositional flow
438 (Kupfer, 1968; Wagner and Jackson, 2011; Jackson et al., 2014); (iii) *Model 3* (Fig. 16c) - the Zechstein
439 Supergroup was deposited in a bathymetrically complex basin, the physiography of which was inherited
440 from the Early Permian rift event. Flooding of the basin by the Zechstein Sea during the Late Permian
441 resulted in halite deposition in high accommodation areas (e.g. underfilled basin centre) during sea-level
442 lowstand and carbonate/anhydrite deposition in low accommodation areas (e.g. overfilled basin margin)
443 during sea-level highstand (cf. Tucker, 1991). In this model, subaerial exposure of the Zechstein
444 Supergroup at the basin margin or on intra-basin structural highs during the Triassic or Middle Jurassic-
445 to-Early Cretaceous may have slightly modified the primary lithology and thickness variations in the unit;
446 and (iv) *Model 4* - the Zechstein Supergroup was deposited in a bathymetrically complex basin, the
447 physiography of which was controlled by syn-depositional (i.e. Late Permian) rift-related normal faulting.
448 In a similar manner to *Model 3*, *Model 4* envisages that halite was deposited in high-accommodation areas
449 during sea-level lowstand and carbonate/anhydrite deposition occurred in low-accommodation areas at
450 the basin margin during sea-level highstands (cf. Tucker, 1991). In this model, variations in the thickness
451 and lithology of the Zechstein Supergroup were simply augmented by syn-depositional faulting (not
452 shown in Fig. 16c).

453 Although post-depositional erosion and dissolution (*Model 1*) undoubtedly impacted on the
454 present thickness and lithology variations in the Zechstein Supergroup, we think it was unlikely to be the
455 dominant control because many of the basin-centre successions contain almost no carbonate and, even
456 when relatively thick salt is fully penetrated, relatively little anhydrite (e.g. 17/12-1R; Fig. 10). This
457 suggests that the successions encountered at the basin margins or on intra-basin structural highs cannot
458 simply represent anhydrite- or carbonate-enriched versions of the basin-centre successions. We also
459 discount preferential flow of halite as being the dominant control on the lithological variations in the
460 Zechstein Supergroup because the thin successions encountered on the basin margin and intra-basin
461 structural highs are not flanked by large salt structures (e.g. 15/9-9 and 16/4-1; Figs 7 and 9). Although

462 Jackson and Lewis (2013) provide evidence for Early Permian rifting and faulting along at least the
463 northern margin of the Egersund Basin, and despite dramatic changes in thickness and lithology occurring
464 in the Zechstein Supergroup across basement-involved normal faults, we have no independent evidence
465 for a regional phase of Late Permian extension, thus making it difficult to discriminate between Models 2
466 and 3.

467

468 **Mechano-stratigraphic controls on structural style development in salt-influenced rift basins**

469

470 Salt has unique rheological properties, being weak under both extension and compression and, most
471 importantly. It is weaker than most other lithologies at significant (>500 m) burial depths and flows like a
472 fluid over geological timescales (e.g. Hudec and Jackson, 2007; Jackson and Hudec, 2017). As a result of
473 these rheological properties, salt can strongly modify the structural style of rift basins (e.g. Stewart et al.,
474 1996, 1997; Clark et al., 1998; Duffy et al., 2013; Wilson et al., 2013; Jackson & Lewis, 2016). For
475 example, salt can impede the vertical (and lateral) propagation of and therefore influence the degree of
476 coupling between, sub- and supra-salt normal faults. Furthermore, activity on basement-restricted, thick-
477 skinned and supra-salt faults can trigger halokinesis by, for example, tilting the salt and triggering thin-
478 skinned, gravity-driven deformation and causing reactive diapirism (e.g. Vendeville and Jackson, 1994).
479 As a result, the structural style of salt-influenced rifts is markedly different to rifts that lack salt in their
480 pre-rift mechano-stratigraphic template.

481 Here we have shown that spatial variations in the thickness and lithology of the evaporite-bearing
482 Zechstein Supergroup control the structural styles that develop during Middle Jurassic-to-Early
483 Cretaceous rifting (see also Lewis et al., 2013; Jackson and Lewis, 2016). Diapirism is common in
484 hangingwall basins, where autochthonous salt was thick and halite-rich (e.g. DZs 3 and 4 of Clark et al.,
485 1998). In contrast, at the basin margins and on intra-basin structural highs, in locations where the
486 Zechstein Supergroup was too thin and/or halite-poor to form large diapirs, salt-detached normal faulting
487 occurs in response to basement-involved faulting and overburden tilting (e.g. DZs 1 and 2 of Clark et al.,
488 1998). Locally, very small minibasins may form, although these are rare. This variability is currently not
489 captured by existing tectono-stratigraphic models largely based on observations from salt-free rifts
490 (Gawthorpe and Leeder, 2000). As a corollary, mapping of supra-salt structural styles may provide
491 insights into salt lithology and thickness in areas where boreholes are lacking or seismic imaging is poor
492 below thick, structurally complex overburden. Our study lends support to the UKCS-derived models of
493 Clark et al. (1998) and Stewart (2007), which are based on sparse, low-to-moderate quality 2D seismic
494 data, and even sparser well controls.

495

496 **Comparison to other saline giants**

497 Very few studies have documented the lithological variations occurring in ‘salt giants’ (*sensu* Hsü, 1972);
498 this may reflect a lack of borehole data with which to directly constrain such variations, or a lack of
499 detailed study on the evaporite-dominated stratigraphic interval in those particular basins. Where borehole
500 data are available, they indicate that lithology variations are strongly linked to the pre- or syn-depositional
501 physiography of the salt basin. For example, the middle Carboniferous-to-Permian, Paradox Basin, Utah,
502 USA is a large (265 km by 190 km), asymmetric, foreland basin that formed during the ancestral Rocky
503 Mountain orogenic event (e.g. Barbeau, 2003; Trudgill *et al.*, 2004; Matthews *et al.*, 2007; Trudgill,
504 2011). Thrust sheet loading and long-wavelength crustal flexure led to the formation of a gently north-
505 eastwards dipping homocline, onto which a thick, evaporite-bearing sequence was deposited (Paradox
506 Formation). Because of the relatively simple basin geometry, somewhat predictable lithological and
507 structural style variations occur. In the basin centre the Paradox Formation is halite-rich, although potash,
508 anhydrite and organic-rich black shales occur. Together, these units are arranged into 29 evaporite-shale
509 cycles documenting periodic flooding and desiccation of the basin (Baars, 1983). In contrast, towards the
510 basin margins, the percentage of halite in the Paradox Formation decreases and the succession becomes
511 dominated by carbonates. Seismic reflection data indicate that the style of salt structures in the Paradox
512 Basin reflect this lateral variation in lithology and inferred rheology of the ‘salt’. For example, large salt
513 diapirs characterise the halite-rich, basin centre locations, whereas the basin margin is relatively
514 undeformed. A similar overall relationship between basin morphology, lithology variations, and structural
515 style are observed in the Santos Basin, offshore Brazil (e.g. De Freitas, 2006; Moreira, 2007; Gamboa *et*
516 *al.*, 2008) and in the Mid-Polish Trough, Poland (e.g. Krzywiec, 2012).

517 Our study from the Norwegian sector of the North Sea Basin indicates that lithology and
518 structural style variations are more complex in salt basins characterised by rapid changes in syn-
519 depositional basin relief. More specifically, the length-scales of lithology and thus structural style change
520 are much shorter (<1 km) in rift basins (e.g. the Northern North Sea) where normal faults are present, in
521 contrast to homoclinal ramp-like relief characterising the distal margins of foreland basins; in the latter,
522 lithology and structural; style changes are more gradual, occurring over several tens of kilometres. We
523 argue that the lack of salt structures on intra-basin structural highs does not simply reflect post-
524 depositional uplift and erosion, but may instead indicate areas where salt tectonics never occurred due to
525 the evaporite-bearing sequence lacking low-viscosity, mobile lithologies (e.g. halite, potash salt). Salt
526 basin morphology is thus a key control on lithology distribution in salt giants, and the resulting spatial

527 variations in the mechanical-stratigraphic of the pre-rift template may directly govern structural styles
528 during subsequent phases of crustal extension (Jackson & Lewis, 2016).

529

530 **CONCLUSIONS**

531

532 Regional 2D seismic reflection and borehole data allowed us to constrain thickness and compositional
533 variations in the Zechstein Supergroup (Upper Permian) in the Norwegian sector of the northern North
534 Sea. We showed that halite, anhydrite, and carbonate, represent the main lithologies within the Zechstein;
535 claystone, sandstone, and potassium salts being present, but volumetrically minor. Based on the
536 proportion of halite, we identified and mapped four intrasalt ‘depositional zones’ (*sensu* Clark et al.,
537 1998), showing that, in general, at the basin margins, the Zechstein is carbonate-dominated, whereas
538 towards the basin centre, it is increasingly halite-dominated. More abrupt changes in composition and
539 thickness also occur, invariably across large, intra-basin normal faults, with thin, carbonate-dominated,
540 footwall successions being juxtaposed with thick, halite-dominated, hangingwall successions; it remains
541 unclear if these variations reflect syn-depositional changes in relief related to flooding of an underfilled
542 presalt (Early Permian) rift, and/or syn-depositional (Late Permian) rift-related faulting. Irrespective of
543 the underlying controls, variations in Zechstein composition and thickness influenced Middle Jurassic-to-
544 Early Cretaceous rift structural style, with diapirism characterising hangingwall basins where salt was
545 thick and halite-rich, and salt-detached normal faulting occurring on basin margins and intra-basin
546 structural highs where the salt was too thin and/or halite-poor to undergo diapirism. We show how
547 suprasalt structural styles may provide insights into salt composition and thickness in areas where
548 boreholes are lacking or seismic reflection imaging is poor. Furthermore, we provide additional evidence
549 that the tectono-stratigraphic development of salt-influenced rifts differs significantly to that of salt-free
550 rifts, with the style of crustal deformation reflecting the contrasting mechanical properties of evaporite
551 and related rock types.

552

553 **ACKNOWLEDGMENTS**

554 This research presented in this paper formed part of the Statoil-funded Salt-Influenced Rift Basins (SIRB)
555 project, which was based at Imperial College, the University of Manchester, and the University of
556 Bergen. We would like to acknowledge the technical input of numerous people based in the Norwegian
557 North Sea South Licenses Team (Stavanger) and in the Research Centre (Bergen). We would also like to
558 acknowledge Schlumberger for providing Petrel to all three institutes. Robin Warner, Aruna Mannie and
559 Matthew Lewis are also thanked for their contribution to elements of the work presented here.

560

561 **REFERENCES**

562

563 BAARS, D.L. & STEVENSON, G.M. (1981) Tectonic evolution of the Paradox basin, Utah and
564 Colorado. In: *Geology of the Paradox Basin* (Ed. by D.L. Wiegand), pp. 23-31. Association of
565 Geologists, Rocky Mount.

566

567 BAARS, D.L. (1983) *The Colorado Plateau, a geologic history*. University of New Mexico Press.

568

569 BARTHOLOMEW, I.D., PETERS, J.M. & POWELL, C.M. (1993) Regional structural evolution of the
570 North Sea: oblique-slip and reactivation of basement lineaments. In: *Petroleum Geology of Northwest*
571 *Europe: Proceedings of the 4th Conference* (Ed. by J.R. Parker), pp. 1109-1122. Geological Society,
572 London.

573

574 BISHOP, D.J. (1996) Regional distribution and geometry of salt diapirs and supra-Zechstein Group faults
575 in the western and central North Sea, *Mar. Petrol. Geol.*, **13**, 355-364.

576

577 BRANTHER, S.R.F. (2003) The East Brae field, blocks 16/03a, 16/03b, UK North Sea. In: *United*
578 *Kingdom Oil and Gas Fields, Commemorative Millennium Volume* (Ed. by J. Gluyas & H.M.
579 Hichens), *Geological Society, London, Memoir* **20**, 191-197.

580

581 BREHM, J.A. (2003) The North and Beinn fields, block 16/7a, UK North Sea. In: *United Kingdom Oil*
582 *and Gas Fields, Commemorative Millennium Volume* (Ed. by J. Gluyas & H.M. Hichens), *Geological*
583 *Society, London, Memoir* **20**, 199-209.

584

585 BROWN, A. (2004) Interpretation of three-dimensional seismic data. AAPG Memoir 42, SEG
586 Investigations in Geophysics, 9.6th edn.

587

588 BURLIGA, S., KOYI, H.A., CHEMIA, Z (2012) Analogue and numerical modelling of salt supply to a
589 diapiric structure rising above an active basement fault. In: *Salt Tectonics, Sediment and*
590 *Prospectivity*. (Ed. by G.I. Alsop, S.G. Archer, A.J. Hartley, N.T. Grant, R. Hodgkinson), *Geol. Soc.*
591 *London Spec. Publ.*, 363, 395–408.

592

593 CARTWRIGHT, J.A., STEWART, S. & CLARK, J. (2001) Salt dissolution and salt-related deformation
594 of the Forth Approaches Basin, UK North Sea. *Mar. Petrol. Geol.*, **18**, 757-778.
595

596 CHERRY, S.T.J. (1993) The interaction of structure and sedimentary process controlling deposition of
597 the Upper Jurassic Brae formation Conglomerate, block 16/17, North Sea. In: *Petroleum Geology of*
598 *Northwest Europe: Proceedings of the 4th Conference* (Ed. by J.R. Parker), pp. 387-400. Geological
599 Society, London.
600

601 CLARK, J.A., STEWART, S.A. & CARTWRIGHT, J.A. (1998) Evolution of the NW margin of the
602 North Permian Basin, UK North Sea. *J. Geol. Soc. of London*, **155**, 663-676.
603

604 COCKINGS, J.H., KESSLER, L.G. II, MAZZA, T.A., & RILEY, L.A. (1992) Bathonian to mid-
605 Oxfordian sequence stratigraphy of the South Viking Graben, North Sea. In: *Exploration Britain:*
606 *Insights for the Next Decade* (Ed. by R.F.P. Hardman), *Geol. Soc. London Spec. Publ.*, **67**, 65–105.
607

608 COWARD, M.P. (1995) Structural and tectonic setting of the Permo-Triassic basins of Northwest
609 Europe. In: *Permian and Triassic Rifting in Northwest Europe* (Ed. by S.A.R. Boldy), **91**, 7-39.
610

611 COWARD, M.P., DEWEY, J.F., HEMPTON, M. & HOLROYD, J. (2003) Tectonic evolution. In: *The*
612 *Millennium Atlas: Petroleum Geology of the Central and Northern North Sea* (Ed. by D. Evans, C.
613 Graham, A. Armour & P. Bathurst), pp17-33. The Geological Society of London, London.
614

615 DAVIES, R., DONNELL, D., BENTHAM, P.N., GIBSON, J.P.C., CURRY, M.R., DUNAY, R.E. &
616 MAYNARD, J.R. (1999) The origina and genesis of major Jurassic unconformities within the triple
617 junction area of the North Sea, UK. In: *Petroleum Geology of Northwest Europe: Proceedings of the*
618 *5th conference* (Ed. by A.J. Fleet & S.A.R. Boldy), pp. 117-131. Geological Society, London.
619

620 DAVISON, I., ALSOP, I. & BIRCH, P. (2000) Geometry and Late-stage structural evolution of Central
621 Graben salt diapirs, North Sea. *Mar. Petrol. Geol.*, **17**, 499-522.
622

623 DE FREITAS, R.T.J. (2006) Ciclos Depositionais Evaporiticos Da Bacia De Santos: Uma Analise
624 Cicloestratigrafica a Partir De Dados De 2 Pocos E De Tracos De Sismica., Universidade Federal do
625 Rio Grande do Sul, Brazil.

626

627 DUFFY, O.B., GAWTHORPE, R.L., DOCHERTY, M. & BROCKLEHURST, S.H. (2013) Mobile
628 evaporite controls on the structural style and evolution of rift basins. *Basin Res.*, 25, 310–330.

629

630 ERRATT, D. (1993) Relationships between basement faulting, salt withdrawal and Late Jurassic rifting,
631 UK Central North Sea. In: *Petroleum Geology of Northwest Europe: Proceedings of the 4th*
632 *Conference* (Ed. by J. R. Parker), pp. 1211-1219. Geological Society, London.

633

634 ERRATT, D., THOMAS, G.M. & WALL G.R.T. (1999) The evolution of the Central North Sea Rift. In:
635 *Petroleum Geology of Northwest Europe: Proceedings of the 5th conference* (Ed by A.J. Fleet &
636 S.A.R. Boldy), pp. 63-82. Geological Society, London.

637

638 EVANS D., ARMOUR, A., BATHURST, P., GAMMAGE, J., SWALLOW, J., GRAHAM, C. &
639 STEWART, H. (2003) *Millennium Atlas: Petroleum Geology of Central & Northern North Sea*.
640 London, The Geological Society of London, 390p.

641

642 FLETCHER, K.J. (2003a) The Central Brae field, blocks 16/07a, 16/07b, UK North Sea. In: *United*
643 *Kingdom Oil and Gas Fields, Commemorative Millennium Volume* (Ed. by J. Gluyas & H.M.
644 Hichens), **20**, 183-190.

645

646 FLETCHER, K.J. (2003b) The South Brae field, blocks 16/07a, 16/07b, UK North Sea. In: *United*
647 *Kingdom Oil and Gas Fields, Commemorative Millennium Volume* (Ed. by J. Gluyas & H.M.
648 Hichens), **20**, 211-221.

649

650 FRASER, S.I., ROBINSON, A.M., JOHNSON, H.D., UNDERHILL, J.R., KADOLSKY, D.G.A.,
651 CONNELL, R., JOHANNESSEN, P. & RAVNAS, R. (2003) Upper Jurassic. In: *The Millennium*
652 *Atlas: Petroleum Geology of the Central and Northern North Sea* (Ed. by D. Evans, C. Graham, A.
653 Armour & P. Bathurst), pp. 157-189. The Geological Society of London, London.

654

655 GAMBÔA, L.A.P., MACHADO, M.A.P., SILVEIRA, D.P., DE FREITAS, J.T.R. & DA SILVA, S.R.P.
656 (2008) Evaporitos Estratificados No Atlantico Sul: Interpretacao Sismica E Controle Tectono-
657 Estratigrafico Na Bacia De Santos. In Mohriak, W., Szatmari, P. & Anjos, S.M.C. Sal: *Geologia e*
658 *Tectonica, Exemplos nas Basicas Brasileiras.*, Beca Edicoes Ltda, Sao Paulo, Brasil, 340-359.

659
660 GLENNIE, K.W., HIGHMAN J., & STEMMERIK, L. (2003) Permian. In: *The Millenium Atlas:*
661 *petroleum geology of the central and northern North Sea* (Ed by D. Evans, C. Graham, A. Armour &
662 P. Bathurst), pp. 91-103. The Geological Society of London, London.
663
664 GOLDSMITH, P.J., HUDSON, G. & VAN VEEN, P. (2003) Triassic. In: *The Millenium Atlas:*
665 *petroleum geology of the central and northern North Sea* (Ed by D. Evans, C. Graham, A. Armour &
666 P. Bathurst), pp. 105-127. The Geological Society of London, London.
667
668 HODGSON, N.A., FARNSWORTH, J. & FRASER, A.J. (1992) Salt-related tectonics, sedimentation and
669 hydrocarbon plays in the Central Graben, North Sea, UKCS. In: *Exploration Britain: Geological*
670 *Insights for the Next Decade*. (Ed. by R.F.P. Hardman), *Geol. Soc. London Spec. Publ.*, **67**, 31–63.
671
672 HUDEC, M.R. & JACKSON, M.P.A. (2007) Terra infirma: Understanding salt tectonics. *Earth- Science*
673 *Reviews*, **82**, 1-28.
674
675 JACKSON, M.P.A., VENDEVILLE, B.C. & ELA-SCHULTZ, D.D. (1994) Structural dynamics of salt
676 systems. *Annual Review of Earth and Planetary Sciences*, **22**, 93-117.
677
678 JACKSON, C.A-L. & LARSEN, E. (2008) Temporal constraints on basin inversion provided by 3D
679 seismic and well data: a case study from the SVG. *Basin Res.*, **20**, 397-417.
680
681 JACKSON, C.A-L. & E. LARSEN (2009) Temporal and spatial development of a gravity-driven normal
682 fault array: Middle–Upper Jurassic, South Viking Graben, northern North Sea. *J. Struct. Geol.*, **31**, p.
683 388 – 402.
684
685 JACKSON, C.A-L., KANE, K.E. & LARSEN, E (2010) Structural evolution of minibasins on the Utsira
686 High, northern North Sea; implications for Jurassic sediment dispersal and reservoir distribution. *Pet.*
687 *Geosci.*, **16**, 105-120.
688
689 JACKSON, C.A-L. & LEWIS M.M, (2016) Structural style and evolution of a salt-influenced rift basin
690 margin: the impact of variations in salt composition and the role of polyphase extension. *Basin*
691 *Research*, **28**, 81-102.

692
693 KANE K.E., C.A-L. JACKSON & E. LARSEN (2010) Normal fault growth and fault-related folding in a
694 salt-influenced rift basin: South Viking Graben, Offshore Norway. *J. Struct. Geol.*, **32** (4), 490-506.
695
696 KNOTT, S.D., BURCHELL, M.T., JOLLEY, E.J. & FRASER, A.J. (1993) Mesozoic to Cenozoic plate
697 reconstructions of the North Atlantic and hydrocarbon plays of the Atlantic margins. In: *Petroleum*
698 *Geology of Northwest Europe: Proceedings of the 4th Conference* (Ed. by J.R. Parker), pp. 953-974.
699 Geological Society, London.
700
701 KNOTT, S.D. (2001) Gravity-driven crustal shortening in failed rifts. *J. Geol. Soc.*, **158**, 193-196.
702
703 KOYI, H., JENYON, M.K. & PETERSON, K. (1993) The effect of basement faulting on diapirism. *J.*
704 *Petrol. Geol.*, **16**, 285-312.
705
706 KRZYWIEC, P. (2012) Mesozoic and Cenozoic evolution of salt structures within the Polish Basin: An
707 overview. In: *Salt Tectonics, Sediment and Prospectivity*. (Ed. by G.I. Alsop, S.G. Archer, A.J.
708 Hartley, N.T. Grant, R. Hodgkinson), Geol. Soc. London Spec. Publ., 363, 381–394.
709
710 LYNGSIE, S.B., THYBO, H. & RASMUSSEN, T.M. (2006) Regional geological and tectonic structures
711 of the North Sea area from potential field modelling. *Tectonophysics*, **413**, 147-170.
712
713 MARSH, N., IMBER, J., HOLDSWORTH, R.E., BROCKBANK, P. & RINGROSE, P. (2009) The
714 structural evolution of the Halten Terrace, offshore Mid-Norway: extensional fault growth and strain
715 localisation in a multi-layer brittle-ductile system. *Basin Res.*, **22**, 195-214.
716
717 MATTHEWS, W.J., HAMPSON, G.J., TRUDGILL, B.D. & UNDERHILL, J.R. (2007) Controls on
718 fluvio-lacustrine reservoir distribution and architecture in passive salt diapir provinces: insights from
719 outcrop analogs. *Am. Assoc. Petrol. Geol. Bull.*, **91**, 1367-1403.
720
721 MILTON, N.J. (1993) Evolving depositional geometries in the North Sea Jurassic rift. In: *Petroleum*
722 *Geology of Northwest Europe: Proceedings of the 4th Conference* (Ed by J.R. Parker), pp. 425-442.
723 Geological Society London.
724

725 MOREIRA, J.L.P., MADEIRA, C., GIL, J.A. & MACHADO, M.A.P. (2007) Bacia De Santos. Bulletin
726 Geociencias Petrobras, 15, 531-549.
727

728 PEGRUM, R.M. & LJONES, T.E. (1984) 15/9 Gamma gas field offshore Norway, new trap type for the
729 North Sea basin with regional structural implications. *AAPG Bull.*, **68**, 874-902.
730

731 PENGE, J., TAYLOR, B., HUCKERBY, J.A. & MUNNS, J.W. (1993) Extension and salt tectonics in the
732 East Central Graben. In: *Petroleum Geology of Northwest Europe: Proceedings of the 4th Conference*
733 (Ed. by J.R. Parker), pp. 1197-1210. Geological Society of London.
734

735 RICHARDSON, N.J., UNDERHILL, J.R. & LEWIS, G. (2005) The role of evaporite mobility in
736 modifying subsidence patterns during normal fault growth and linkage, Halten Terrace, Mid-Norway.
737 *Basin Res.*, **17**, 203–223.
738

739 ROBERTS, A.M., YIELDING, G., KUSZNIR, N.J., WALKER, I.M. & DORN-LOPEZ, D. (1995)
740 Quantitative analysis of Triassic extension in the Northern Viking Graben. *J. Geol. Soc.*, **152**, 15-26.
741

742 ROWAN, M.G. & WEIMER, P. (1998) Salt-Sediment interaction, Northern Green Canyon and Edwing
743 Bank (Offshore Louisiana), Northern Gulf of Mexico. *AAPG Bull.*, **82**, 1055-1082.
744

745 SCHLUMBERGER (1985) Log interpretation charts, Schlumberger Publication.
746

747 SCHLUMBERGER (1989a) Log interpretation, principles and applications, Schlumberger Educational
748 Services.
749

750 SCHLUMBERGER (2009) Log Interpretation Charts. 2009 Edition, Schlumberger Publication.
751

752 SHELLEY, D.C. & LAWTON, T.F. (2005) Sequence stratigraphy of tidally-influenced deposits in a salt-
753 withdrawal minibasin: Upper sandstone member of the Potrerillos Formation (Paleocene), La Popa
754 basin Mexico. *Am. Assoc. Petrol. Geol. Bull.*, **89**, 1157-1179.
755

756 SMITH, R.I., HODGSON, N., & FULTON, M. (1993) Salt control on Triassic reservoir distribution,
757 UKCS Central North Sea. In: *Petroleum Geology of Northwest Europe: Proceedings of the 4th*

758 *Conference* (Ed by J.R. Parker), pp. 547-557. Geological Society London.
759
760 STEWART, S.A. (in press) Hormuz salt distribution and influence on structural style in NE Saudi Arabia.
761 *Petroleum Geoscience*, doi.org/10.1144/petgeo2017-011.
762
763 STEWART, S.A. & COWARD, M.P. (1995) Synthesis of salt tectonics in the southern North Sea, UK.
764 *Mar. Petrol. Geol.*, **12**, 457-475.
765
766 STEWART, S.A., HARVEY, M.J., OTTO, S.C. & WESTON, P.J. (1996) Influence of salt on fault
767 geometry: examples from the UK salt basins. In: *Salt Tectonics* (Ed. by Alsop G.I., Blundell D.J.,
768 Davison I.) *Geol. Soc. Spec. Publ.*, 100, 175–202.
769
770 STEWART, S.A. & CLARK, J.A. (1999) Impact of salt on the structure of the Central North Sea
771 hydrocarbon fairways. In: *Petroleum Geology of Northwest Europe: Proceedings of the 5th*
772 *Conference* (Ed by A. J. Fleet & S.A.R. Boldy), pp. 179-200. Geological Society London.
773
774 STEWART, S.A. (2007) Salt tectonics in the North Sea Basin: a structural style template for seismic
775 interpreters. In: *Deformation of the Continental Crust: The Legacy of Mike Coward* (Ed. by A.C. Ries,
776 R.W.H. Butler & R.H. Graham). *Geol. Soc. London Spec. Publ.*, **272**, 361-396.
777
778 SØRENSEN, S., MORIZOT, H. & SKOTTHEIM, S. (1992) A tectonostratigraphic analysis of the
779 southeast Norwegian North Sea Basin. In: *Structural and Tectonic Modelling and its Application to*
780 *Petroleum Geology: Proceedings of the Norwegian Petroleum Society Workshop* (Ed. by R.M. Larsen,
781 H. Brekke, B.T. Larsen & E. Talleraas). Amsterdam, Elsevier, 19-42.
782
783 TAYLOR, J.C.M. (1990) Upper Permian-Zechstein. In: *Introduction to the Petroleum Geology of the*
784 *North Sea* (Ed. by K.W. Glennie, 3rd Edition). Blackwell Scientific Publications, 153-190.
785
786 THOMAS, D.W. & COWARD, M.P. (1996) Mesozoic regional tectonics and South Viking Graben
787 formation; evidence for localized thin- skinned detachments during rift development and inversion.
788 *Mar. Petrol. Geol.*, **13**, 149-177.
789

790 TRUDGILL, B., BANBURY, N. & UNDERHILL, J. (2004) Salt evolution as a control on structural and
791 stratigraphic systems: northern Paradox foreland basin, SE Utah, USA. In: *Salt Sediment Interactions*
792 *and hydrocarbon Prospectivity: Proceedings of 24th Annual Gulf Coast Section SEPM Foundation*
793 *Bob F. Perkins research conference* (Ed. by P.J. Post, D.L. Olson, K.T. Lyons, S.L. Palmes, P.F.
794 Harrison & N.C. Rosen), pp 669-700.
795
796 TRUDGILL, B.D. (2011) Evolution of salt structures in the northern Paradox Basin: controls on evaporite
797 deposition, salt wall growth and supra-salt stratigraphic architecture. *Basin Res.*, **23**, 208–238.
798
799 UNDERHILL, J.R., & PARTINGTON, M.A. (1993) Jurassic thermal doming and deflation in the North
800 Sea: implications of the sequence stratigraphic evidence. In: *Petroleum Geology of Northwest Europe:*
801 *Proceedings of the 4th Conference* (Ed. by J.R. Parker), pp. 337-345. Geological Society, London.
802
803 WARREN, J. (1999) *Evaporites: Their Evolution and Economics*. Blackwell Science, Oxford. 438 pp.
804
805 WILLIAMS, G.D. (1993) Structural models for the evolution of the North Sea area. In: *Petroleum*
806 *Geology of Northwest Europe: Proceedings of the 4th conference* (Ed. by J.R. Parker), pp. 1083-1093.
807 Geological Society of London.
808
809 WILSON, P., ELLIOTT, G.M., GAWTHORPE, R.L., JACKSON, C.A.-L., MICHELSEN, L. & SHARP,
810 I.R. (2013) Geometry and segmentation of an evaporite-detached normal fault array: the southern
811 Bremstein Fault Complex, offshore mid-Norway. *J. Struct. Geol.*, **51**, 74–91.
812
813 WITHJACK, M.O. & CALLAWAY, S. (2000) Active normal faulting beneath a salt layer: an
814 experimental study of deformation patterns in the cover sequence. *AAPG Bull.*, **84**, 627-651.
815
816 ZANELLA, E. & COWARD, M.P. (2003) Structural framework. In: *The Millenium Atlas: petroleum*
817 *geology of the central and northern North Sea* (Ed. by D. Evans, C. Graham, A. Armour & P.
818 Bathurst), pp. 45-59. The Geological Society of London.
819
820 ZIEGLER, P.A. (1990) Tectonic and paleogeographic development of the North Sea rift system. In:
821 *Tectonic Evolution of the North Sea Rifts* (Ed. by D. Blundell & A.D. Gibbs), pp. 1-36. Oxford
822 Clarendon Press, Oxford.

823

824 ZIEGLER, P.A. (1992) Geodynamic of rifting and implications for hydrocarbon habitat, *Tectonophysics*,
825 **215**, 221-253.

826

827 **FIGURE CAPTIONS**

828

829 **Fig. 1.** Simplified structural basemap of the study area indicating the position of major basement-involved
830 normal faults, sub-basins and intra-basin structural highs. FGS=Fladen Ground Spur; SVG=South Viking
831 Graben; WGG=Witch Ground Graben; SB=Sleipner Basin; UH=Utsira High; LD=Ling Depression;
832 SH=Sele High; AG=Åsta Graben; EB=Egersund Basin; SP=Stavanger Platform; LN=Lista Nose. The
833 seismic and borehole dataset used in this study is shown. The regional geographical setting of the North
834 (NPB) and South (SPB) Permian basins is shown in the inset map.

835

836 **Fig. 2.** Composite stratigraphic column for the study area. The regional tectono-stratigraphic
837 significance of the various stratigraphic units is indicated (modified from Jackson and Larsen, 2009).

838

839 **Fig. 3.** (a) Map showing the principal lithologies in the Zechstein Supergroup (Upper Permian) along the
840 northwestern margin of the NPB (UK sector of the Central Graben) and their relationship to the main
841 basement-involved structural elements (modified from Stewart, 2007). Four DZs are depicted (1-4),
842 which are differentiated based on their proportion of halite (Clark *et al.*, 1998). Areas of syn-salt (i.e. Late
843 Permian) and immediately post-salt (i.e. Triassic) salt flow are indicated. The red box represents the area
844 considered in our study. (b) Schematic section showing the idealized lateral lithology variability observed
845 between the centre and the margin of an evaporite basin (based on the west margin of the Southern
846 Permian Basin; see Taylor, 1990). Four DZs corresponding to those shown in (a) and which are defined
847 by varying proportions of halite, are recognised.

848

849 **Fig. 4.** Density (RHOB) vs. sonic (DT) cross-plot illustrating the petrophysical expression of the
850 evaporite and non-evaporite lithologies recovered in cuttings from the Zechstein Supergroup. For the
851 location of boreholes see Fig. 1. Note the strong (anhydrite) to very strong (halite) differentiate between
852 evaporite and non-evaporite lithologies. 'Ideal' values (see Schlumberger, 2009) for RHOB and DT are
853 indicated by a black dot with a red (halite) or blue (anhydrite) outer boundary.

854

855 **Fig. 5.** (a) Sonic (DT) vs. gamma-ray (GR) and (b) density (RHOB) vs. gamma-ray (GR) cross-plot
856 illustrating the petrophysical expression of claystone and carbonate recovered in cutting from the
857 Zechstein Supergroup. For the location of boreholes see Fig. 1. Note the strong overlap between these two
858 non-evaporite lithologies.

859

860 **Fig. 6.** Regional Zechstein Supergroup isochron based on mapping of 2D seismic profiles shown in Fig.
861 1. The present depositional/erosional limit of the Zechstein Supergroup is shown, in addition to the
862 locations of major basement-involved normal faults and key boreholes. See the caption for Fig. 1 for the
863 abbreviations for key structural elements.

864

865 **Fig. 7.** Stratigraphic panel (a) and corresponding interpreted seismic profile (b) across the South Viking
866 Graben, Utsira High, Sleipner Terrace and Ling Graben. The stratigraphic panel illustrates the lithological
867 variability between basin centre (i.e. South Viking Graben and Ling Depression) and basin margin (i.e.
868 Utsira High, Sleipner Terrace) locations. The stratigraphic panel is flattened on the top of the Zechstein
869 Supergroup and the lithologies defined in the panel are based on cuttings data. The seismic profile
870 illustrates the structural setting of the wells and their relationships to salt structures. The location of the
871 profile is shown in Fig. 1. GBFZ=Graben Boundary Fault Zone.

872

873 **Fig. 8.** Stratigraphic panel (a) and corresponding interpreted seismic profile (b) across the Sleipner
874 Terrace and Ling Graben. The stratigraphic panel illustrates the lithological variability between basin
875 centre (i.e. western part of the Ling Graben; 16/8-2) and basin margin (i.e. Sleipner Terrace and eastern
876 part of the Ling Graben; 16/9-1) locations. The stratigraphic panel is flattened on the top of the Zechstein
877 Supergroup and the lithologies defined in the panel are based on cuttings data. The seismic profile
878 illustrates the structural setting of the wells and their relationships to salt structures. The location of the
879 profile is shown in Fig. 1.

880

881 **Fig. 9.** Stratigraphic panel (a) and corresponding interpreted seismic profile (b) across the eastern margin
882 of the South Viking Graben. The stratigraphic panel illustrates the lithological variability observed along
883 the basin margin. The stratigraphic panel is flattened on the top of the Zechstein Supergroup and the
884 lithologies defined in the panel are based on electrofacies characterisation (see Fig. 4 and text for further
885 details). The seismic profile illustrates the structural setting of the wells and their relationships to salt
886 structures. The location of the profile is shown in Fig. 1.

887

888 **Fig. 10.** Stratigraphic panel (a) and corresponding interpreted seismic profile (b) across the Ling Graben,
889 Sele High and Åsta Graben. The stratigraphic panel illustrates the lithological variability observed
890 between the basin centre (i.e. Ling and Åsta Graben) and an intra-basin structural high (i.e. Sele High).
891 The stratigraphic panel is flattened on the top of the Zechstein Supergroup and the lithologies defined in
892 the panel are based on electrofacies characterisation (see Fig. 4 and text for further details). The seismic
893 profile illustrates the structural setting of the wells and their relationships to salt structures. The location
894 of the profile is shown in Fig. 1.

895

896 **Fig. 11.** Seismic (a) and geoseismic (b) sections across the eastern margin of the Ling Graben and the
897 western margin of the Sele High; in this position, the boundary between the two structural domains is not
898 fault controlled, and is instead defined by a broadly W- to SW-dipping ramp. This profile covers an area
899 where the Zechstein Supergroup is thought to be relatively halite rich (DZ3 of Clark et al., 1998). The
900 location of the profile is shown in Fig. 1.

901

902 **Fig. 12.** Seismic (a) and geoseismic (b) sections across the eastern margin of the Ling Graben and the
903 western margin of the Sele High; in this position, the boundary between the two structural domains is
904 defined by a relatively large-displacement (600 ms TWT), basement-involved normal fault (F1) (cf. Fig.
905 11). This profile covers an area where the Zechstein Supergroup is thought to pass from being relatively
906 halite-rich in a deep basin setting (i.e. the Ling Depression; DZ3 of Clark et al., 1998), to being relatively
907 halite-poor on the basin margin (i.e. the Sele High). Note that the development of thin-skinned, salt-
908 detached normal faults on the Sele High suggests some halite is present, thus this area may represent DZ2
909 of Clark et al. (1998), rather than DZ1. The location of the profile is shown in Fig. 1.

910

911 **Fig. 13.** Seismic (a) and geoseismic (b) sections across the eastern margin of the Ling Graben, the
912 southern Sele High, and the western Egersund Basin; in this position, the eastern and western boundaries
913 of the Sele High are defined by relatively large-displacement (300-1500 ms TWT), basement-involved
914 normal faults (F1 and F3). This profile covers an area where the Zechstein Supergroup is thought to pass
915 from being relatively halite-rich in deep basin settings (i.e. the Ling Depression and Egersund Basin;
916 DZ3-4 of Clark et al., 1998), to being relatively halite-poor on the basin margin (i.e. the Sele High). Note
917 that the development of relatively small diapirs and shallow minibasins on the Sele High suggests some
918 halite is present, thus this area may represent DZ2 of Clark et al. (1998), rather than DZ1. The location of
919 the profile is shown in Fig. 1.

920

921 **Fig. 14.** Stratigraphic panel (a) and corresponding interpreted seismic profile (b) across the eastern part of
922 the Egersund Basin and the Lista Nose. The stratigraphic panel illustrates the lithological variability
923 observed near the basin margin. The stratigraphic panel is flattened on the top of the Zechstein
924 Supergroup and the lithologies defined in the panel are based on electrofacies characterisation (see Fig. 4
925 and text for further details). The seismic profile illustrates the structural setting of the wells and their
926 relationships to salt structures. The location of the profile is shown in Fig. 1. Note that 10/7-1, which
927 appears to penetrate the lower flank of a diapir, is projected into the section and actually penetrates the
928 immediate footwall of a basin-bounding fault (see Fig. 15).

929

930 **Fig. 15.** Regional map showing the basin-scale distribution of DZs (*sensu* Clark et al., 1998), a proxy for
931 bulk lithology, in the Zechstein Supergroup. In the UK sector, the map is based on data published by
932 Clark et al. (1998) and Stewart (2007); data presented in this study is used to constrain the map in the
933 Norwegian sector. Note that boundaries between domains, especially within the deep basin (e.g. Egersund
934 Basin, South Viking Graben, Ling Depression) and flanking ramps are uncertain and undoubtedly
935 gradational; these boundaries are thus shown as dashed rather than solid lines. Where domain boundaries
936 are fault-controlled, they are likely more abrupt.

937

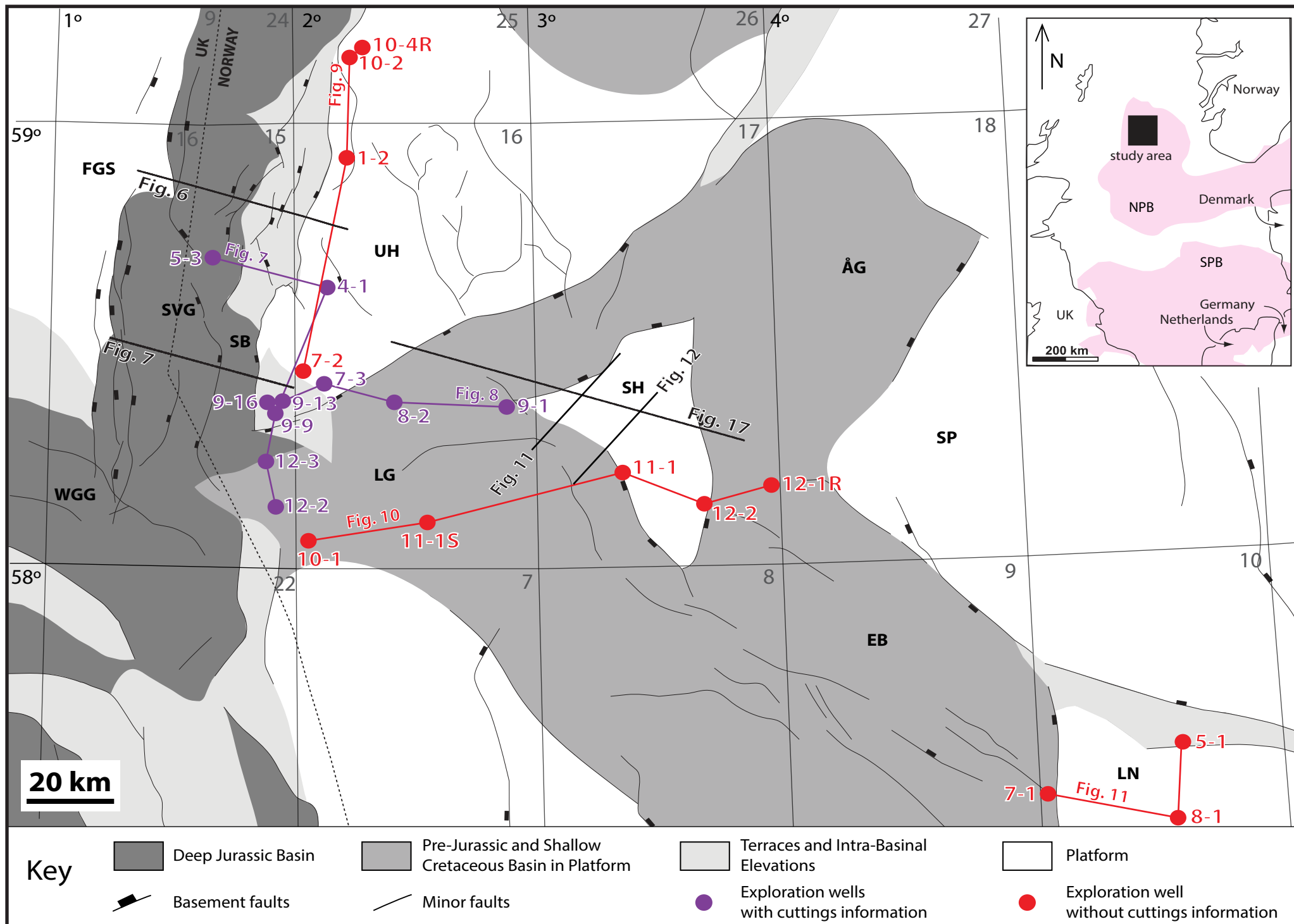
938 **Fig. 16.** Four end-member models that may account for the thickness and lithology variations observed in
939 the Zechstein Supergroup (see also Jackson and Lewis, 2013). (A) Model 1 – thickness and lithology
940 variations driven by post-depositional tectonics (e.g. normal faulting and regional thermal uplift) results
941 in halite dissolution and the relative enrichment in non-halite lithologies at the basin margins and on intra-
942 basin structural highs. Thicker, more halite-rich succession preserved in fault hangingwalls. (B) Model 2
943 – thickness and lithology variations driven by post-depositional flow of a heterogeneous Zechstein
944 Supergroup (i.e. anhydrite-dominated basin margin, halite-dominated basin centre), with flow being
945 strongly partitioned (i.e. mobile halite preferentially expelled from the basin margin into flanking salt
946 structures, resulting in local enrichment of non-halite lithologies in areas where Zechstein Supergroup is
947 thin). (C) Models 3 and 4 – thickness and lithology variations driven by pre- (Model 3) and/or syn-
948 (Model 4) depositional tectonics (e.g. normal faulting and regional thermal uplift). Halite deposition in
949 high accommodation areas (e.g. basin centre) during sea-level lowstand and carbonate/anhydrite
950 deposition in low accommodation areas (e.g. basin margin) during sea-level highstand (cf. Tucker, 1991).
951 In Model 4, variations in the thickness and lithology of the Zechstein Supergroup were simply augmented
952 by syn-depositional faulting. T1-3=sea-level.

953

954 **Table 1.** Summary of the boreholes used in this study. GR=gamma ray; DT=sonic velocity;
955 RHOB=density. See text for full discussion.

956

957 **Table 2.** Petrophysical characteristics of evaporite and non-evaporite lithologies encountered in the
958 Zechstein Supergroup based on borehole cuttings and literature values from Rider and Kennedy (2011).



System		SOUTH VIKING GRABEN, UTSIRA HIGH, LING DEPRESSION			EGERSUND BASIN, SELE HIGH				
		Group	Formation	Tectono-stratigraphic significance	Group	Formation	Tectono-stratigraphic significance		
Cretaceous	Upr.	Chalk	Tor	post-rift	Shetland	Tor	post-rift		
			Hod			Hod			
			Blodøks						
	Lwr.	Cromer Knoll	Rødby		inversion	Cromer Knoll	Rødby	syn-rift	
Sola			Sola						
Åsgard			Åsgard						
Upr.	Viking	Draupne	syn-rift	Boknfjord		Flekkiefjord	syn-rift		
		Heather				Sauda			
		Hugin				Tau			
Mid.	Vestland	Sleipner		BJU	Vestland	Egersund		syn-rift	
						Sandnes			
Triassic		Hegre			Skagerrak	minibasin fill/ rafted blocks			Hegre
			Smith Bank		Smith Bank				
Permian	Upr.	Zechstein	pre-rift		evaporite-rich source of salt-tectonic structures/ intrastratal detachment	Zechstein	pre-rift		evaporite-rich source of salt-tectonic structures/ intrastratal detachment
	Lwr.	Rotliegendes		Auk				Rotliegendes	

Figure 2

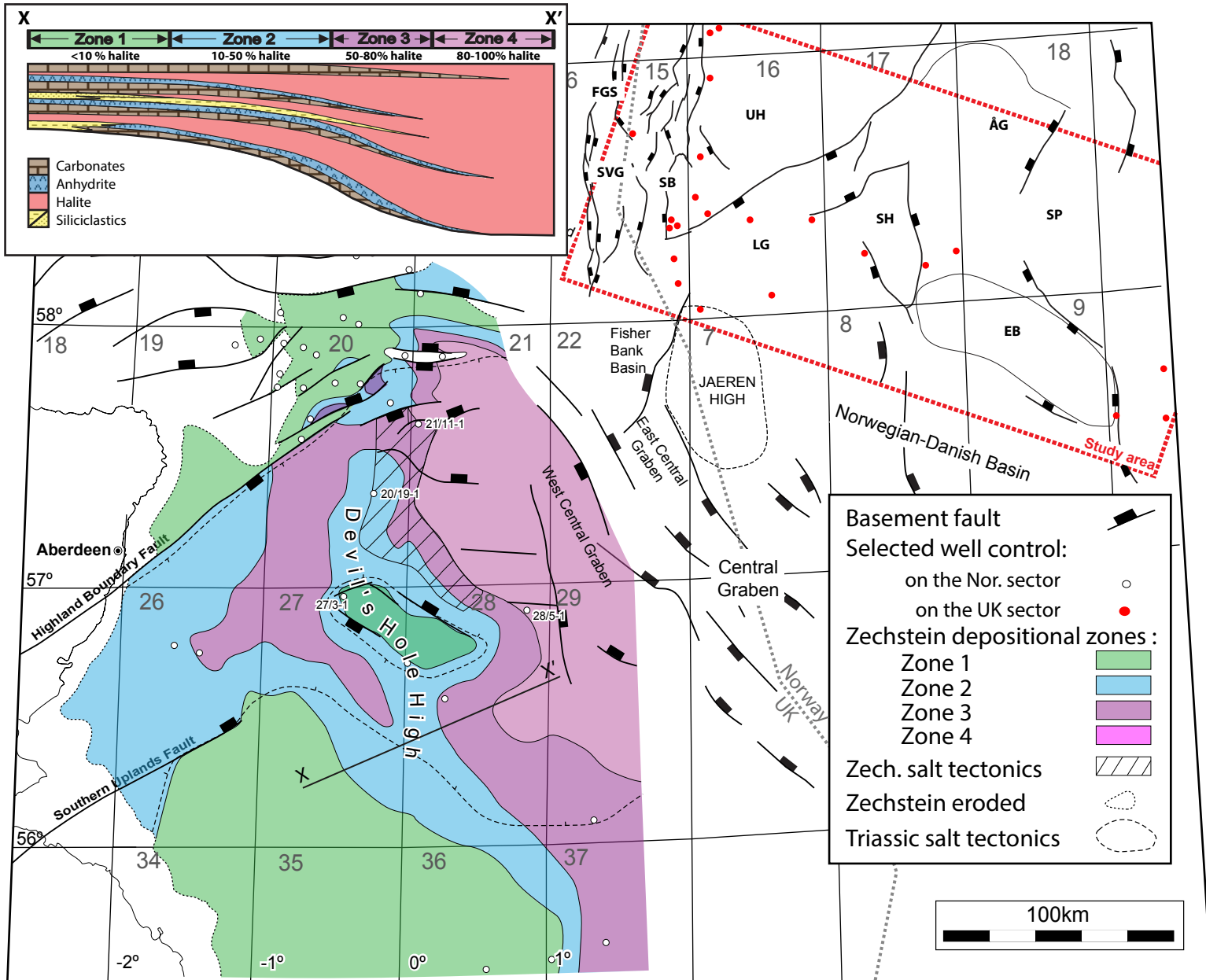


Figure 3

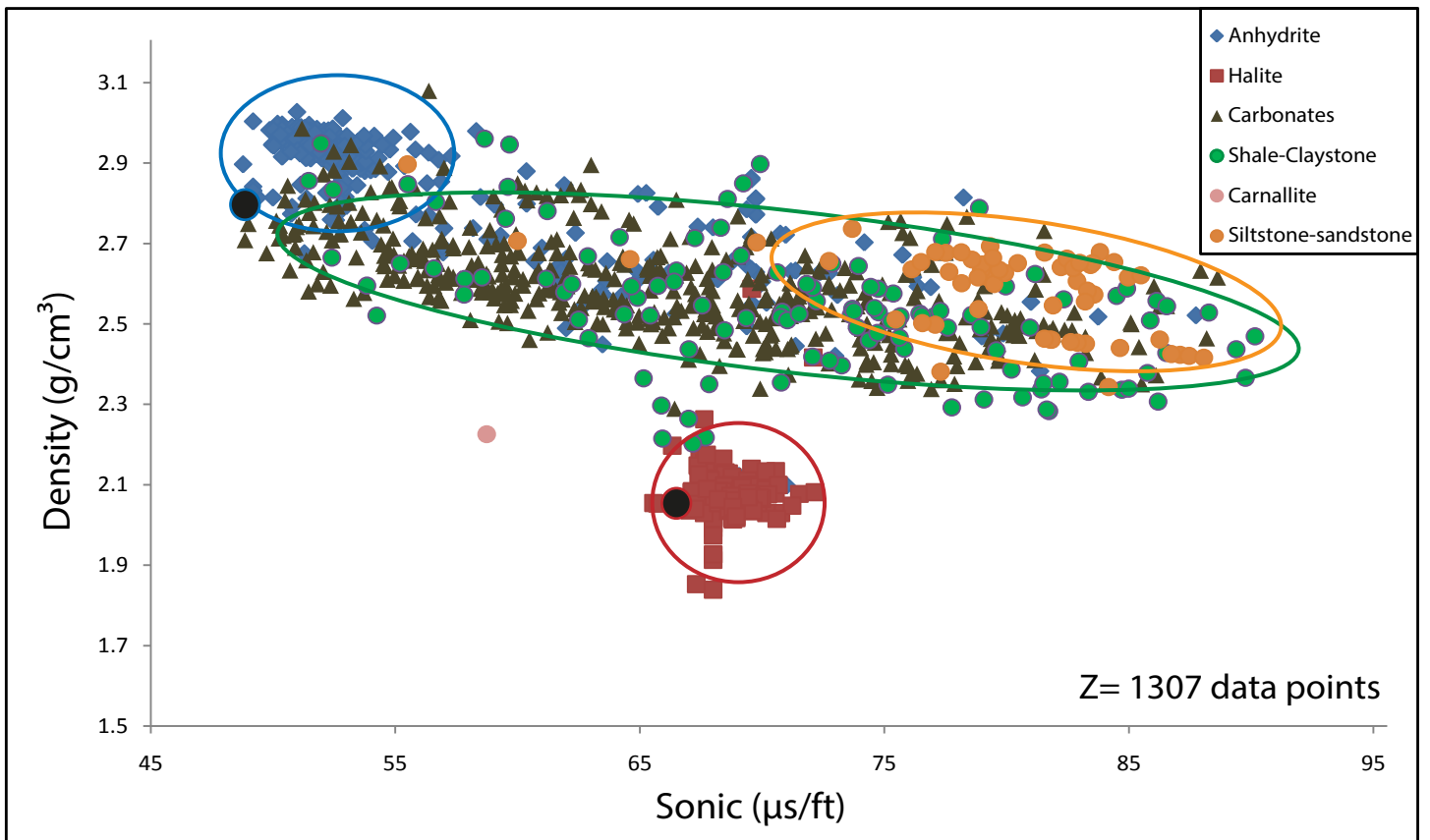


Figure 4

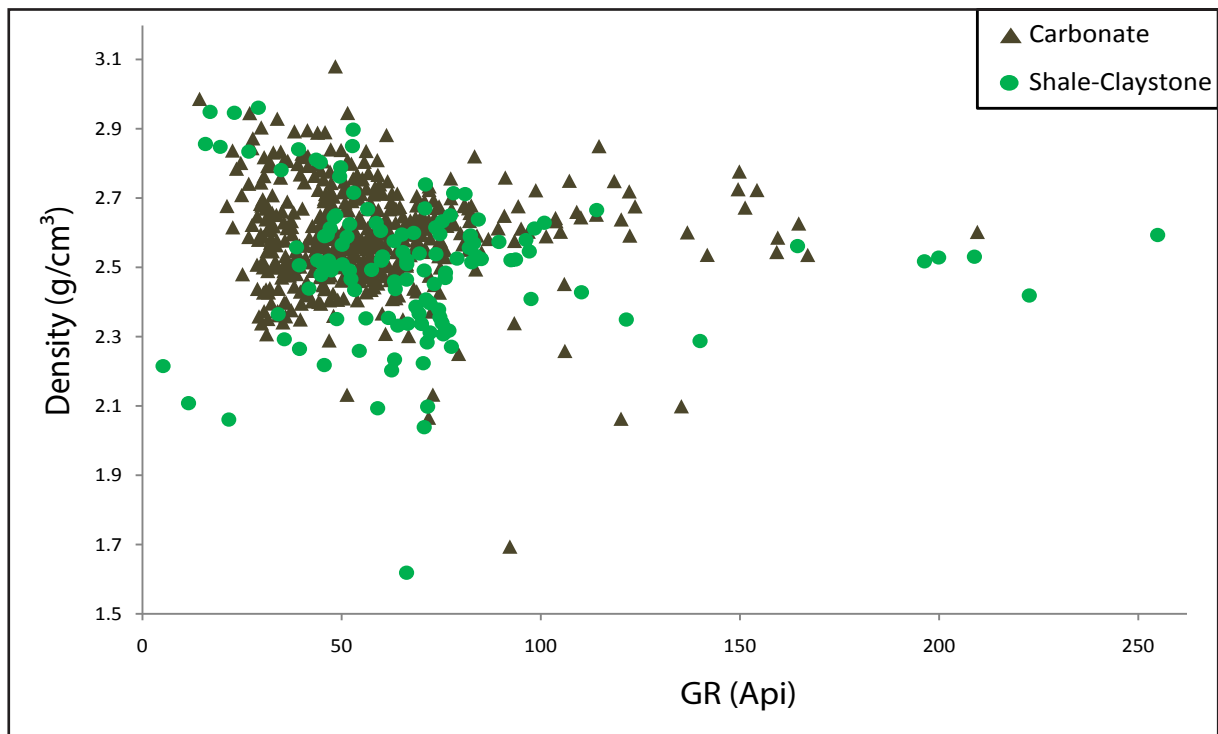
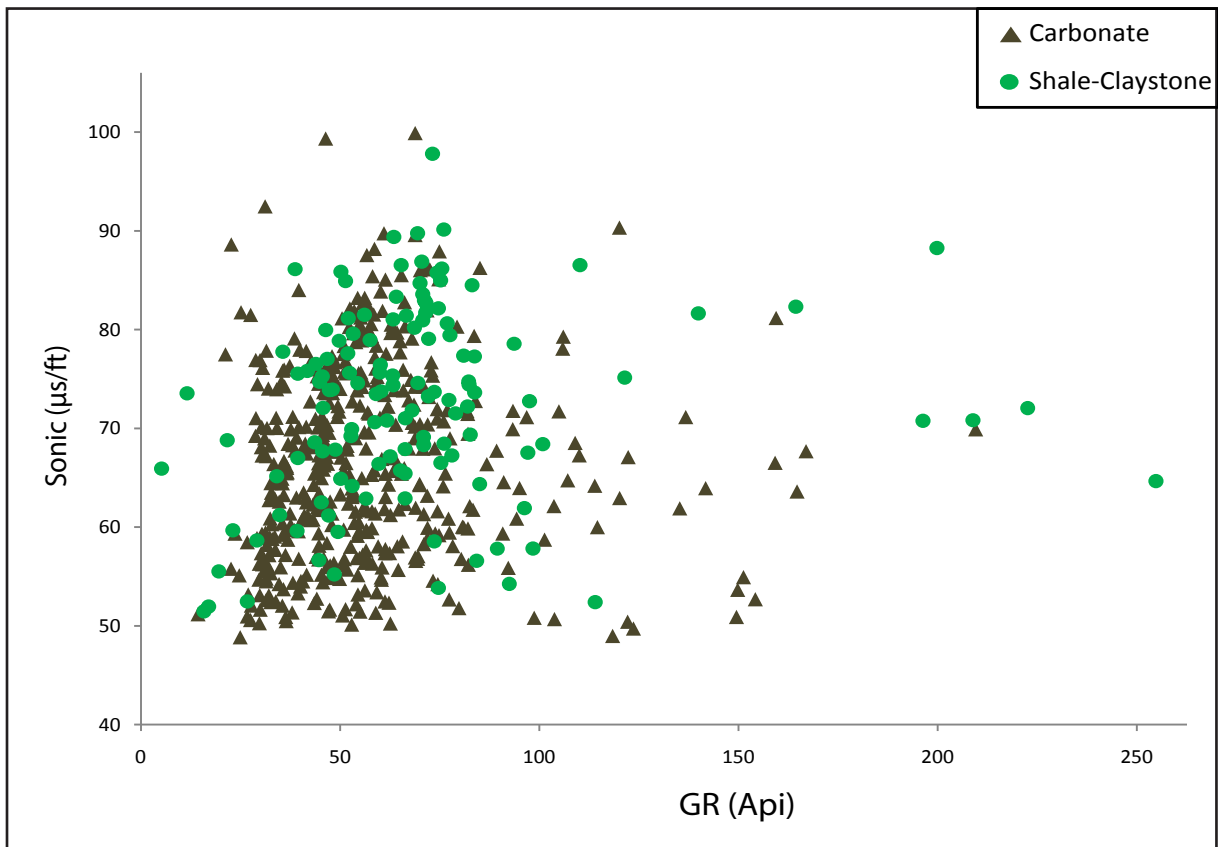


Figure 5

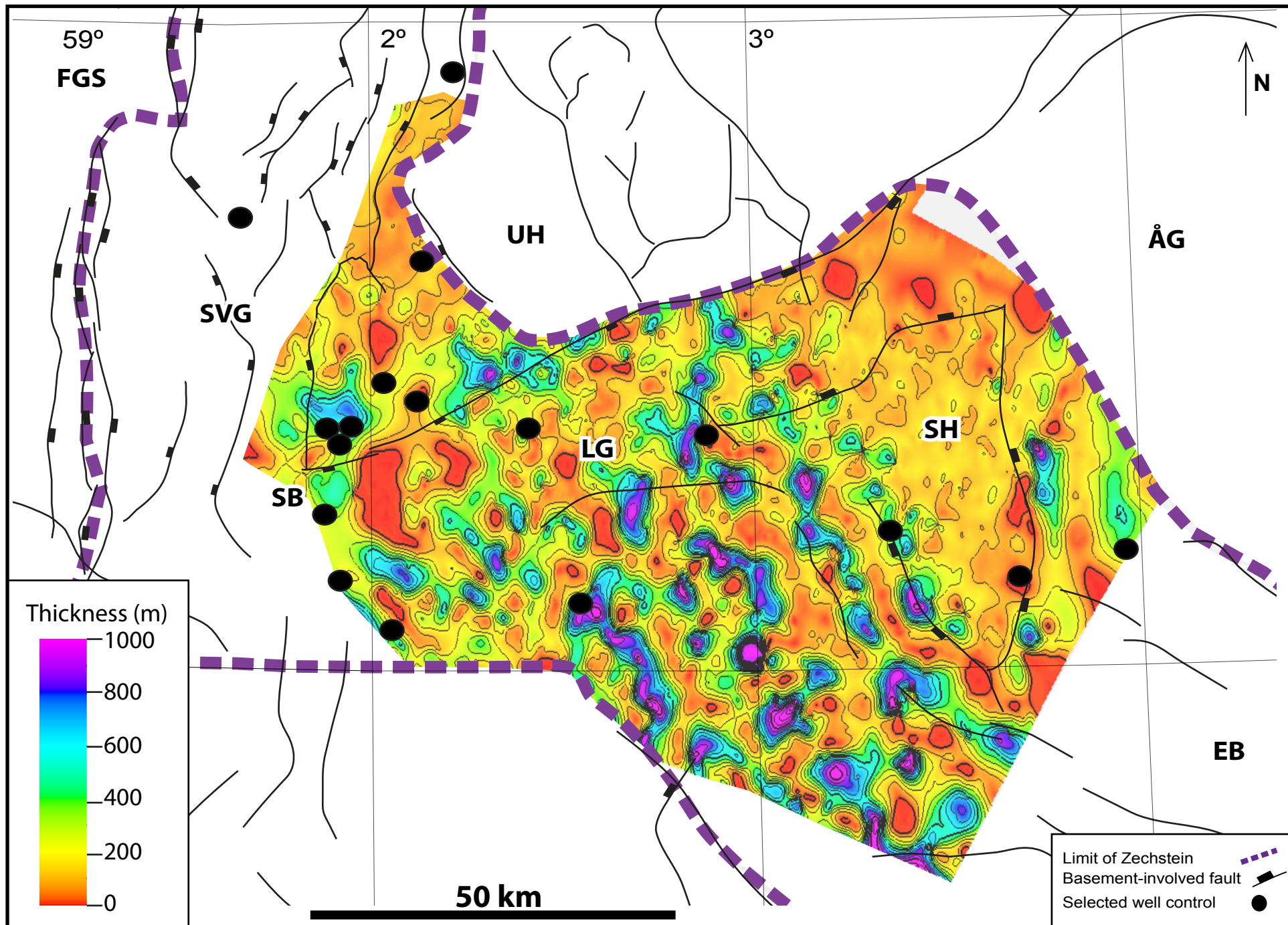


Figure 6

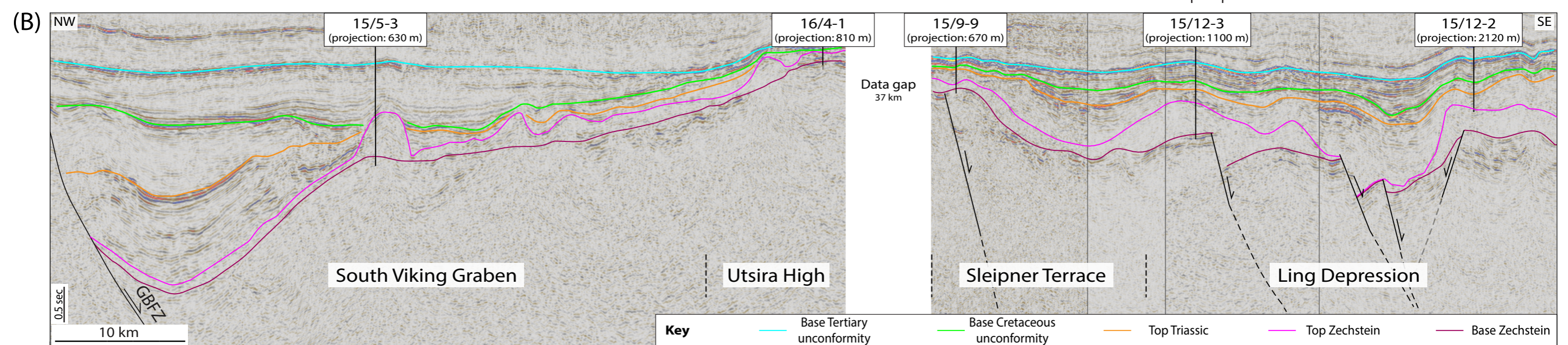
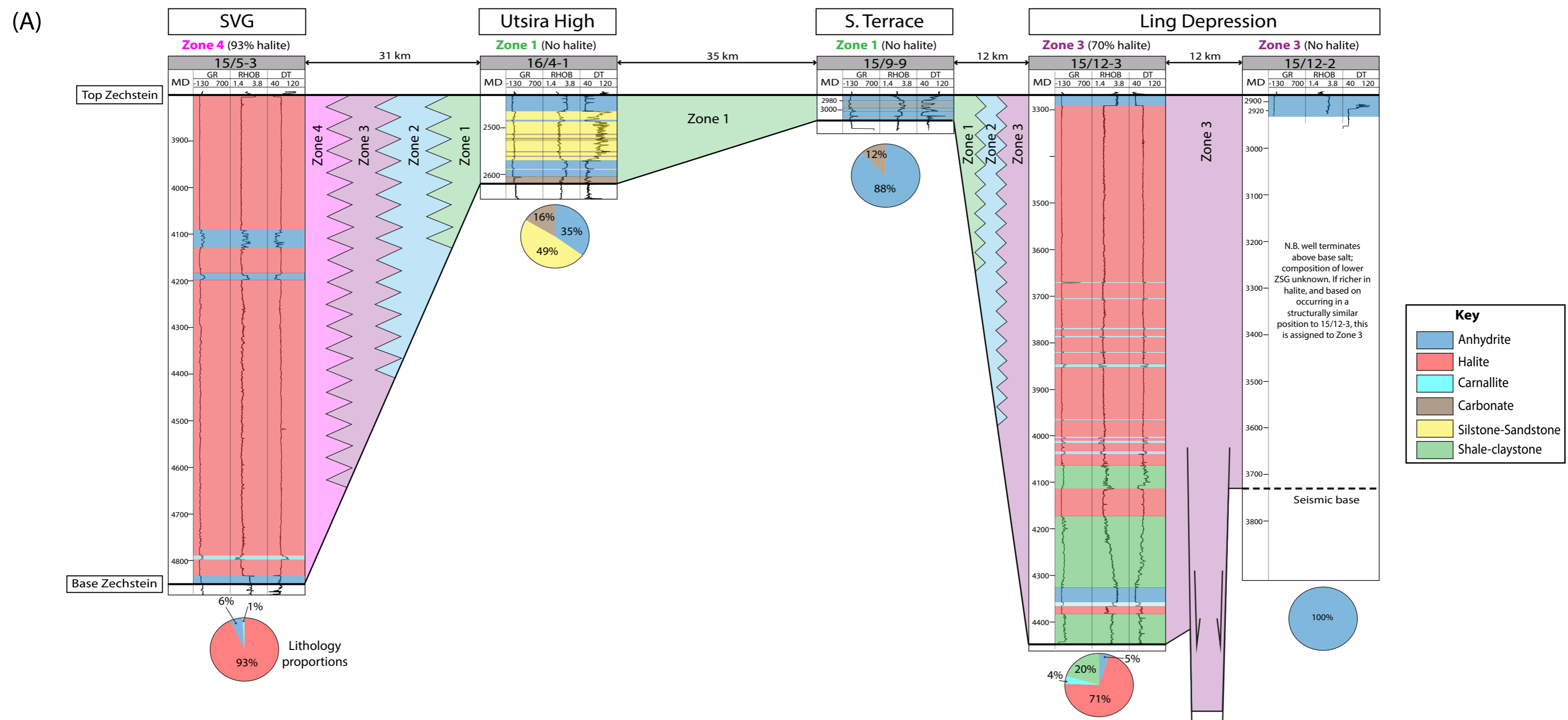
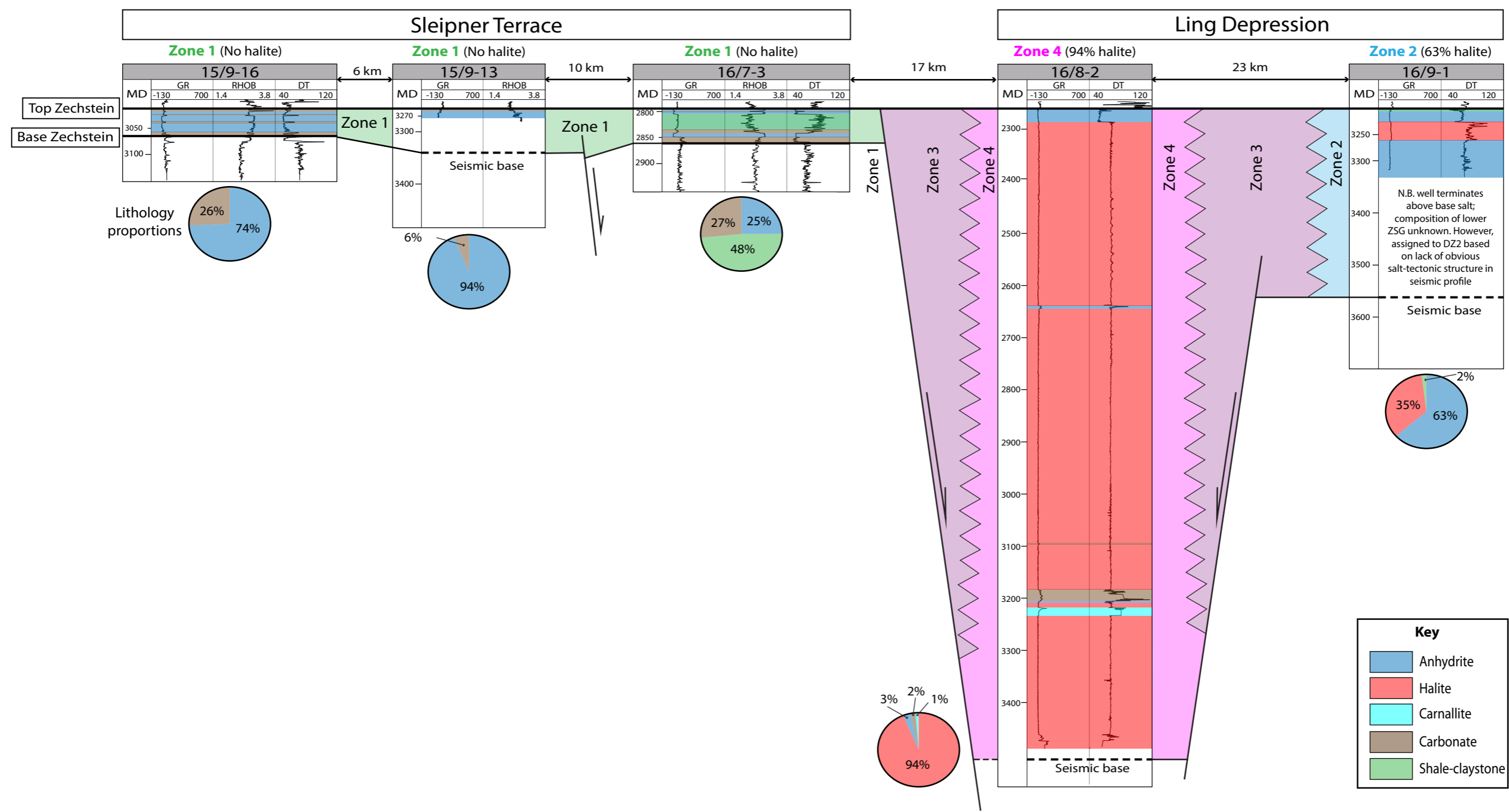


Figure 7

(A)



(B)

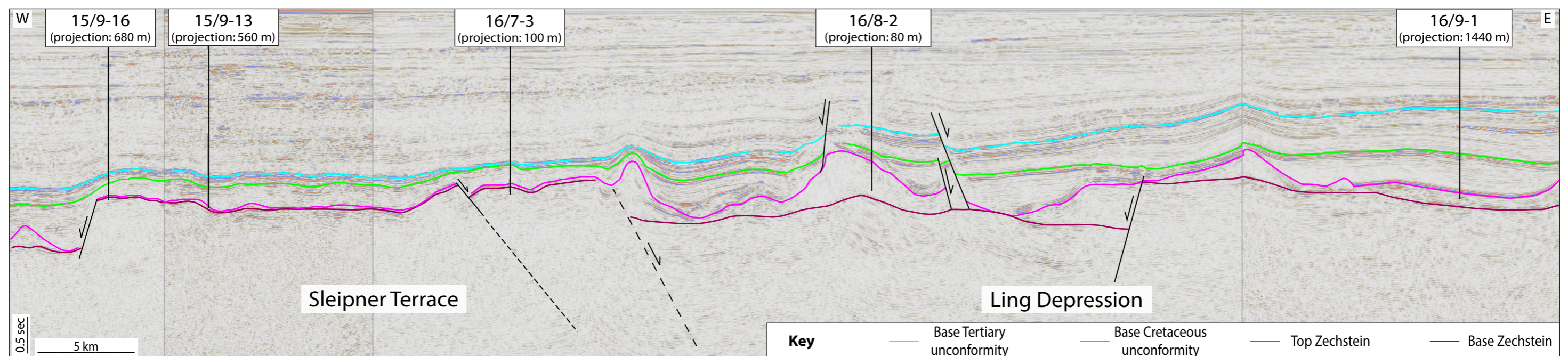


Figure 8

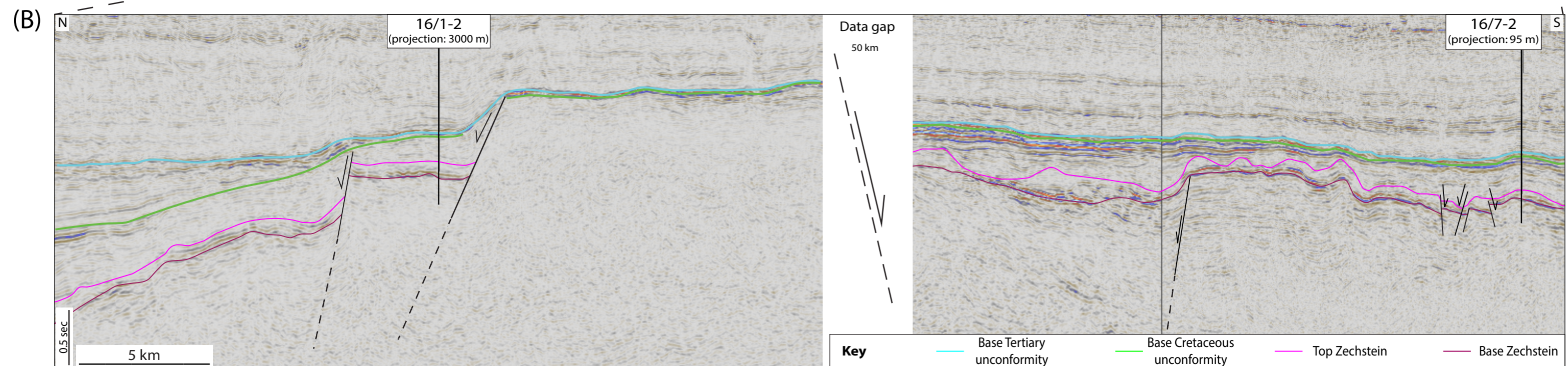
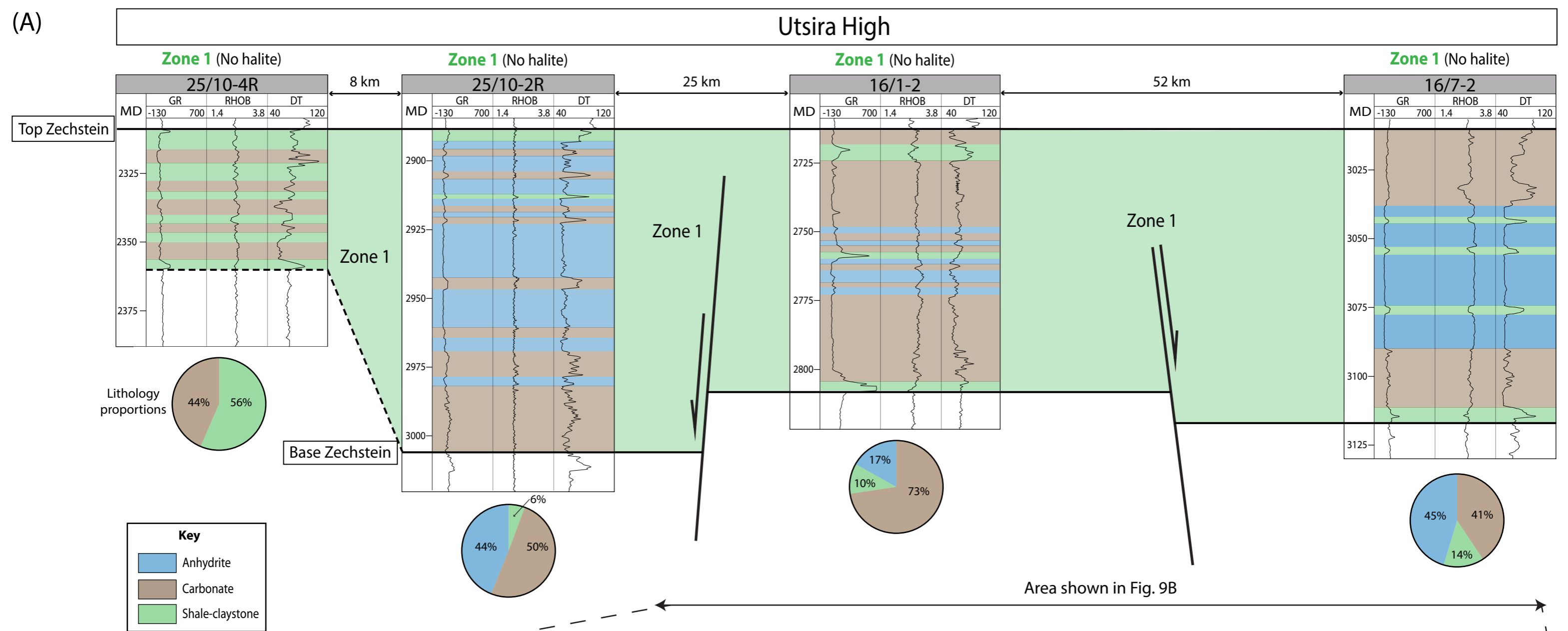


Figure 9

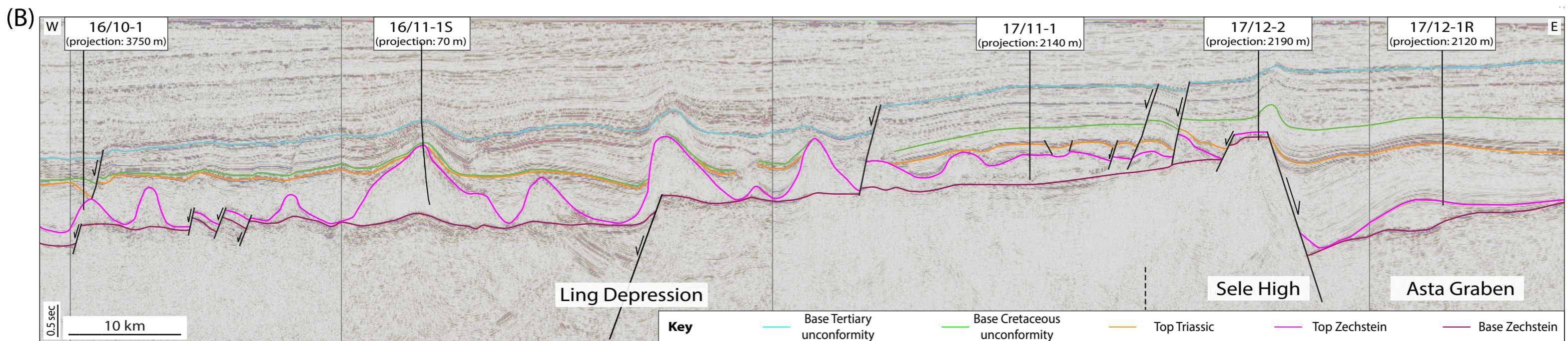
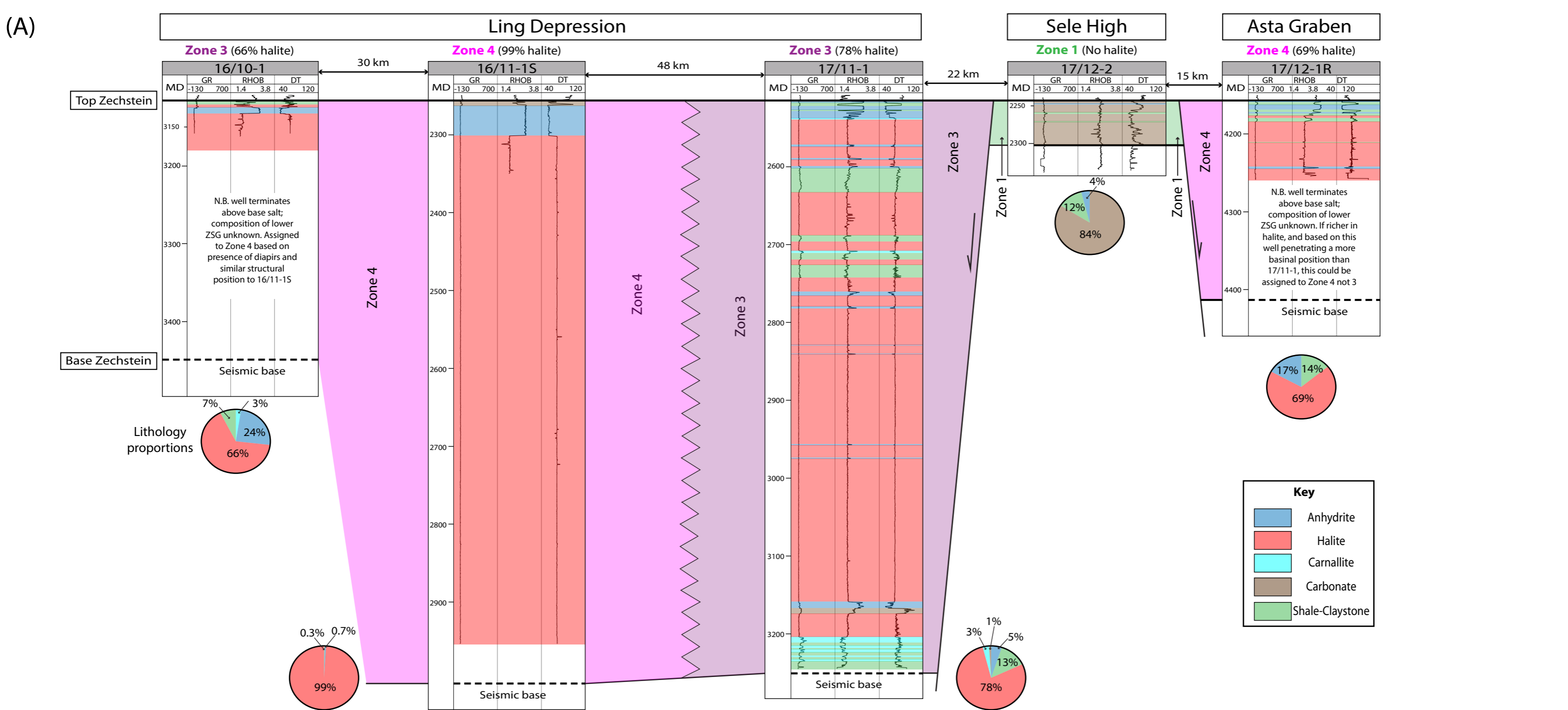


Figure 10

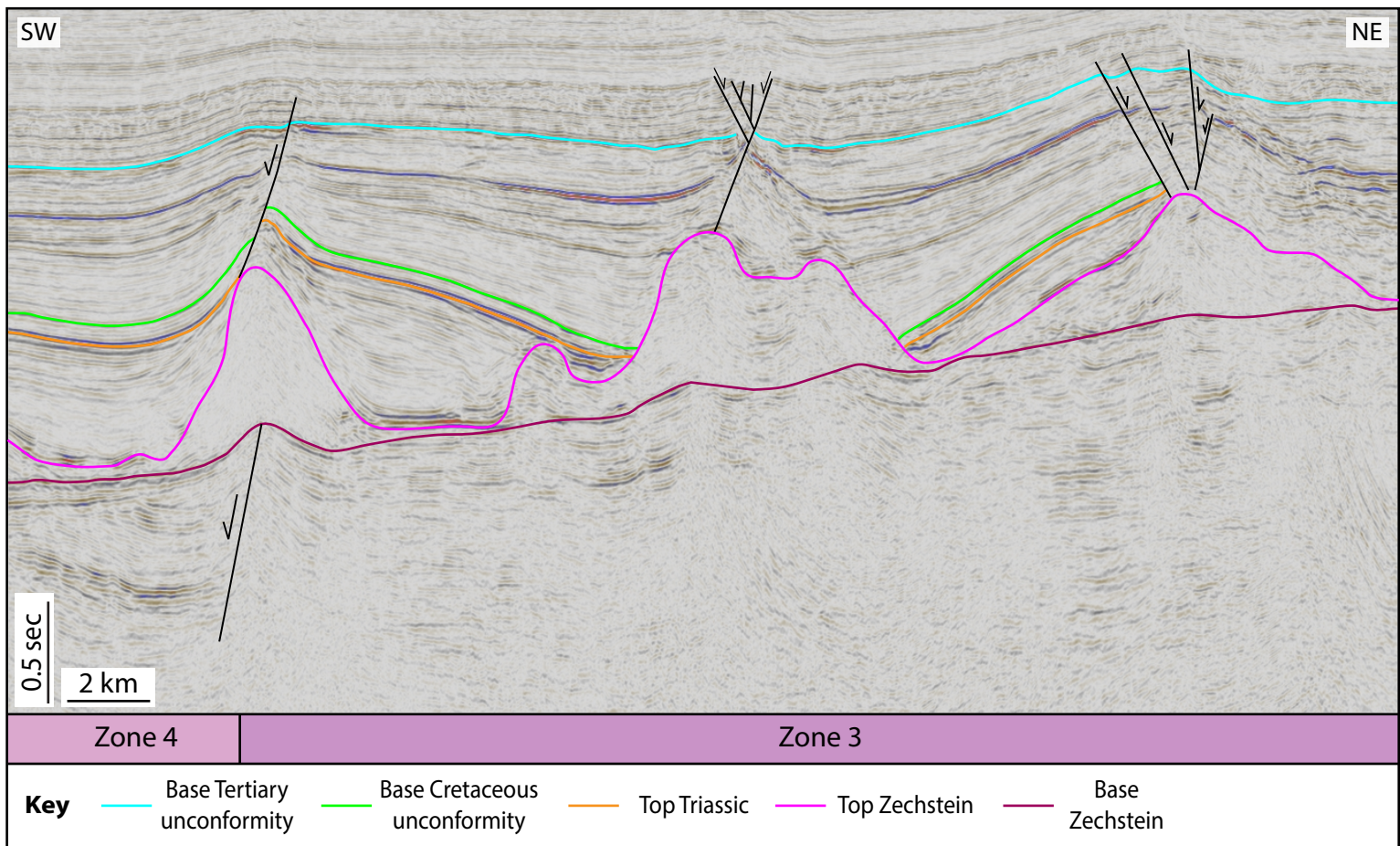
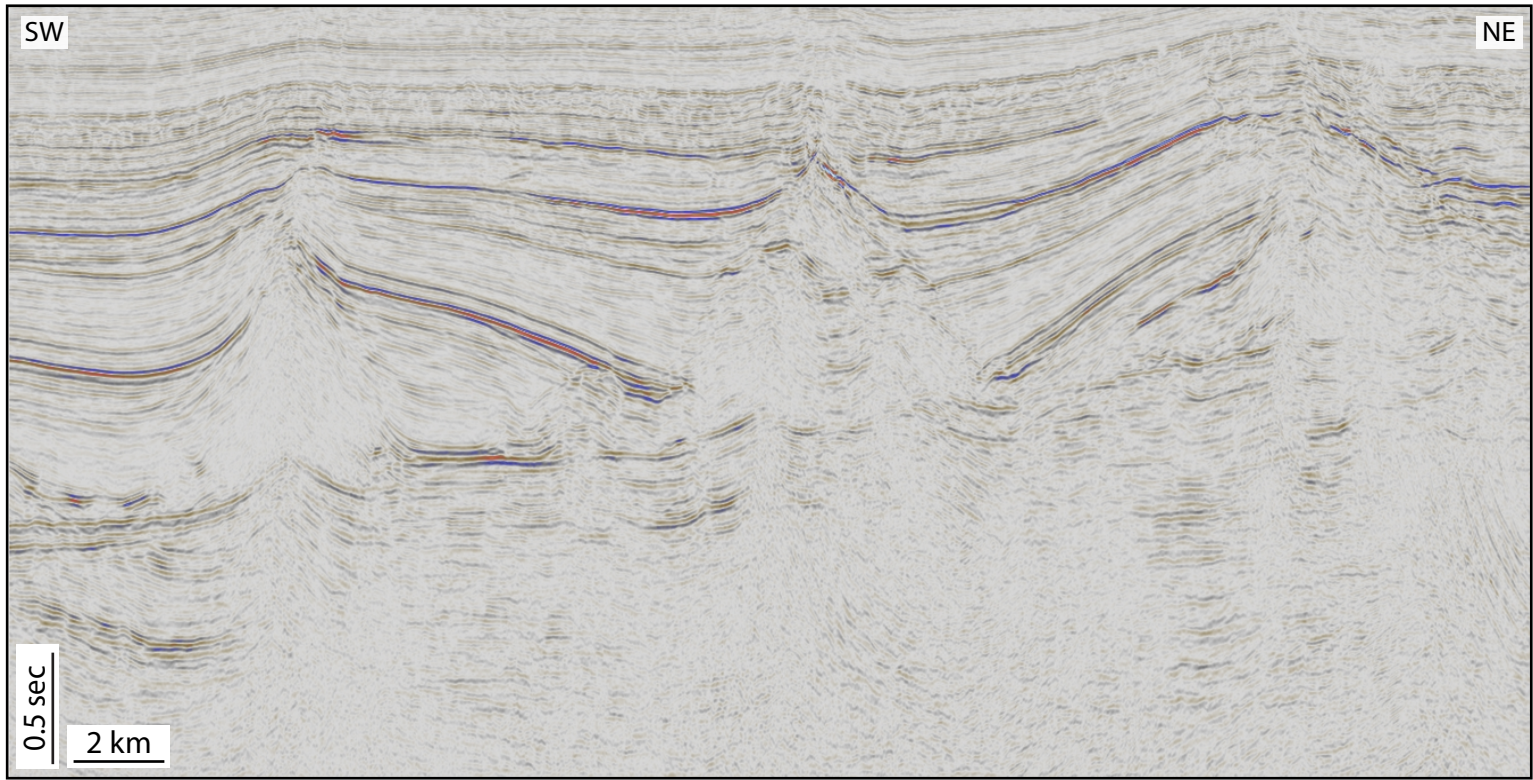


Figure 11

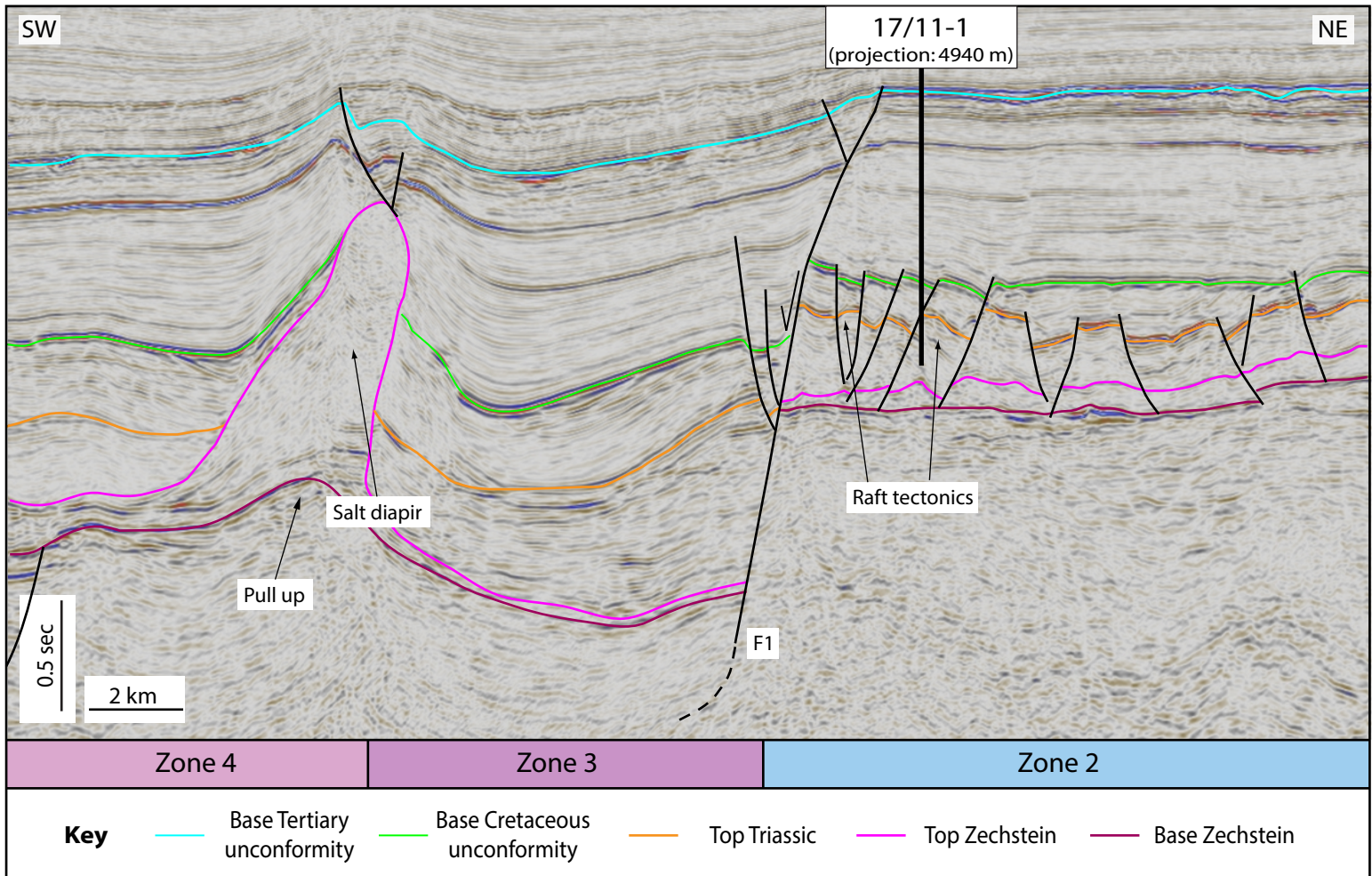
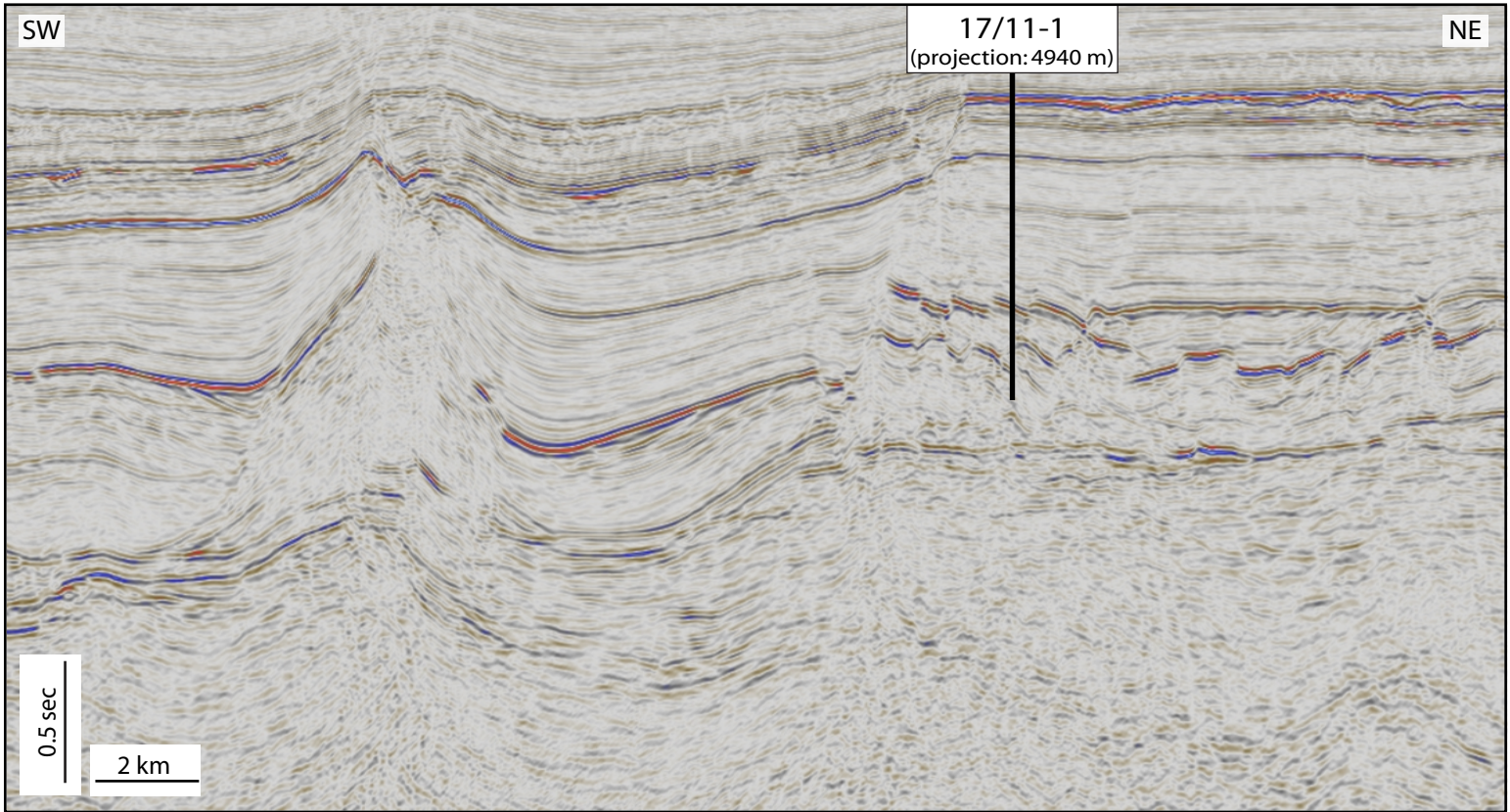


Figure 12

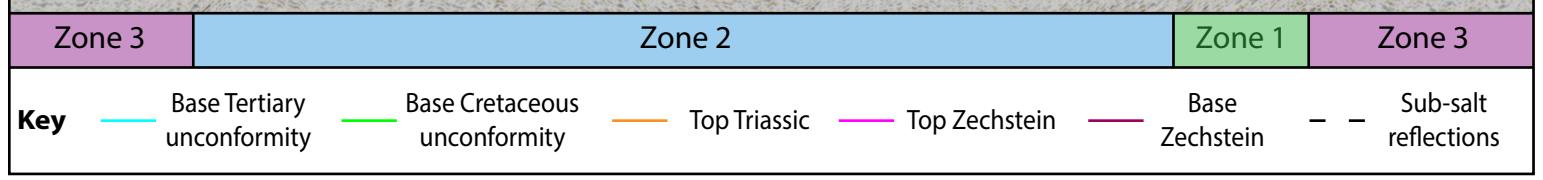
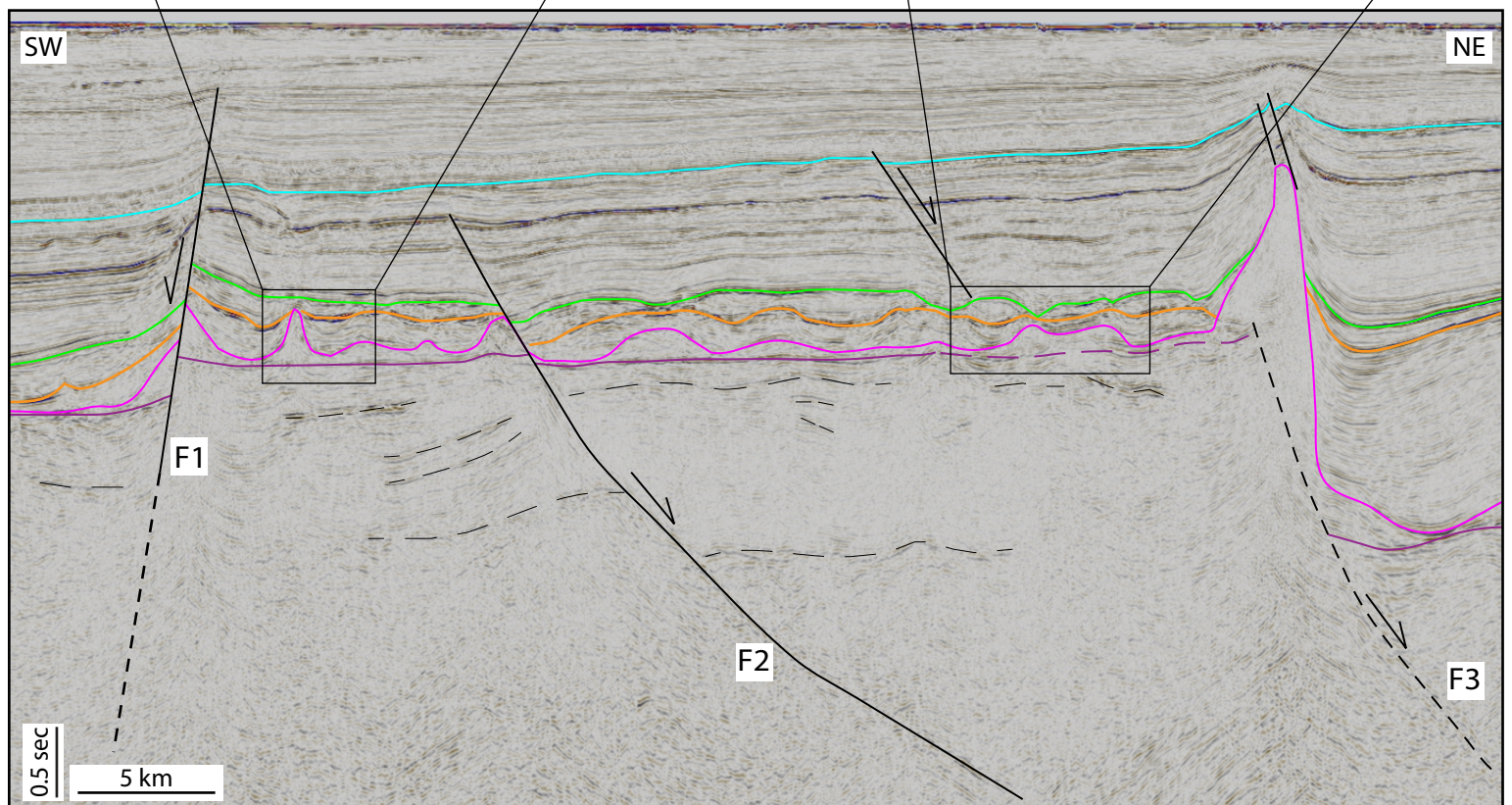
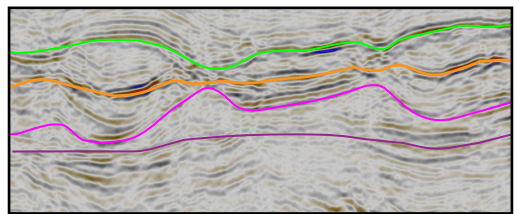
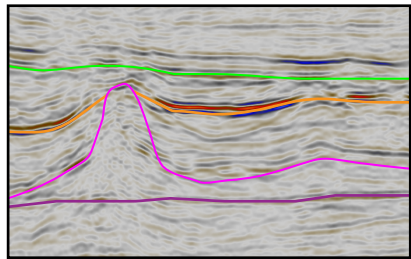
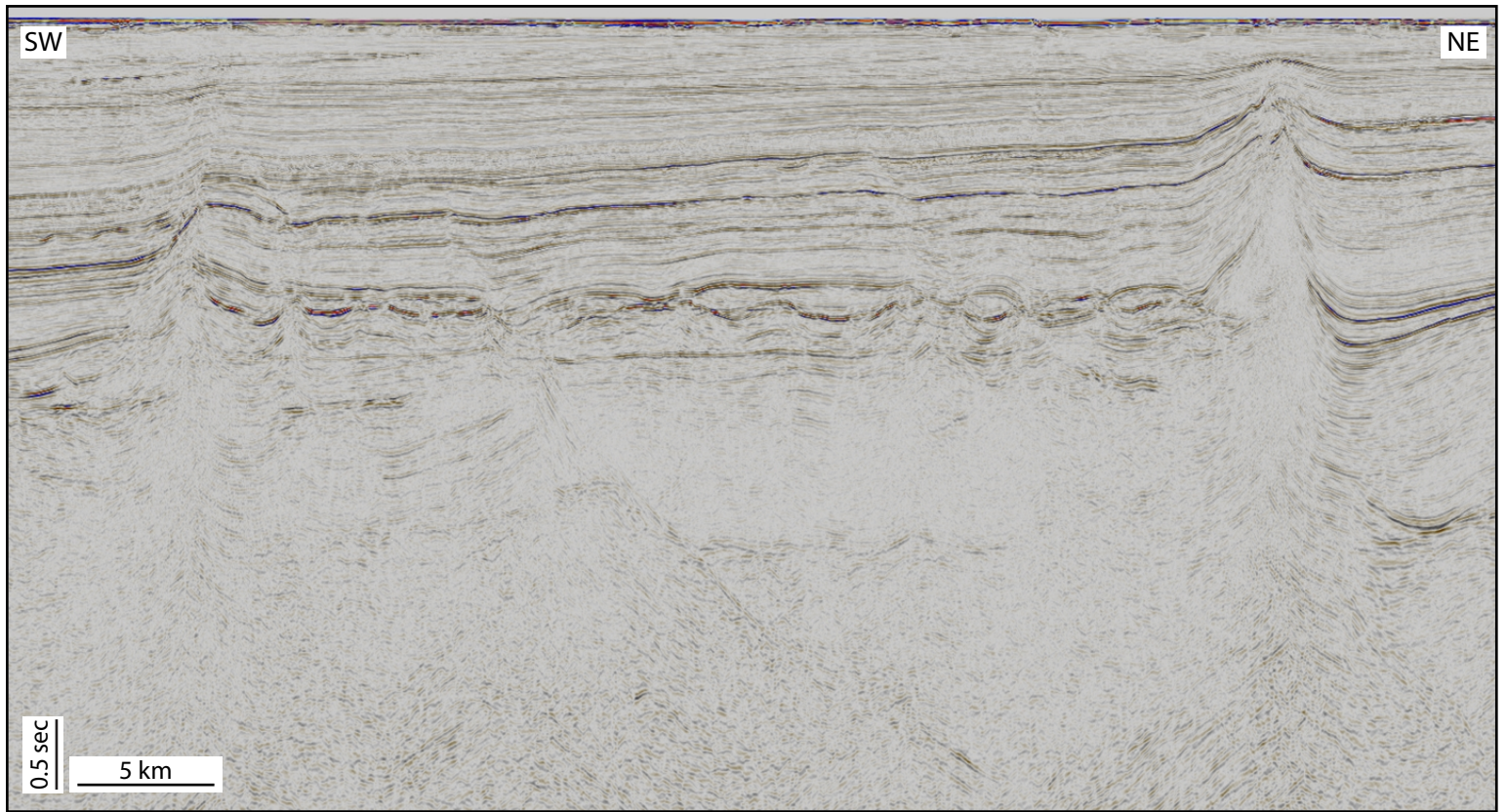


Figure 13

Lista Fault Block Complex

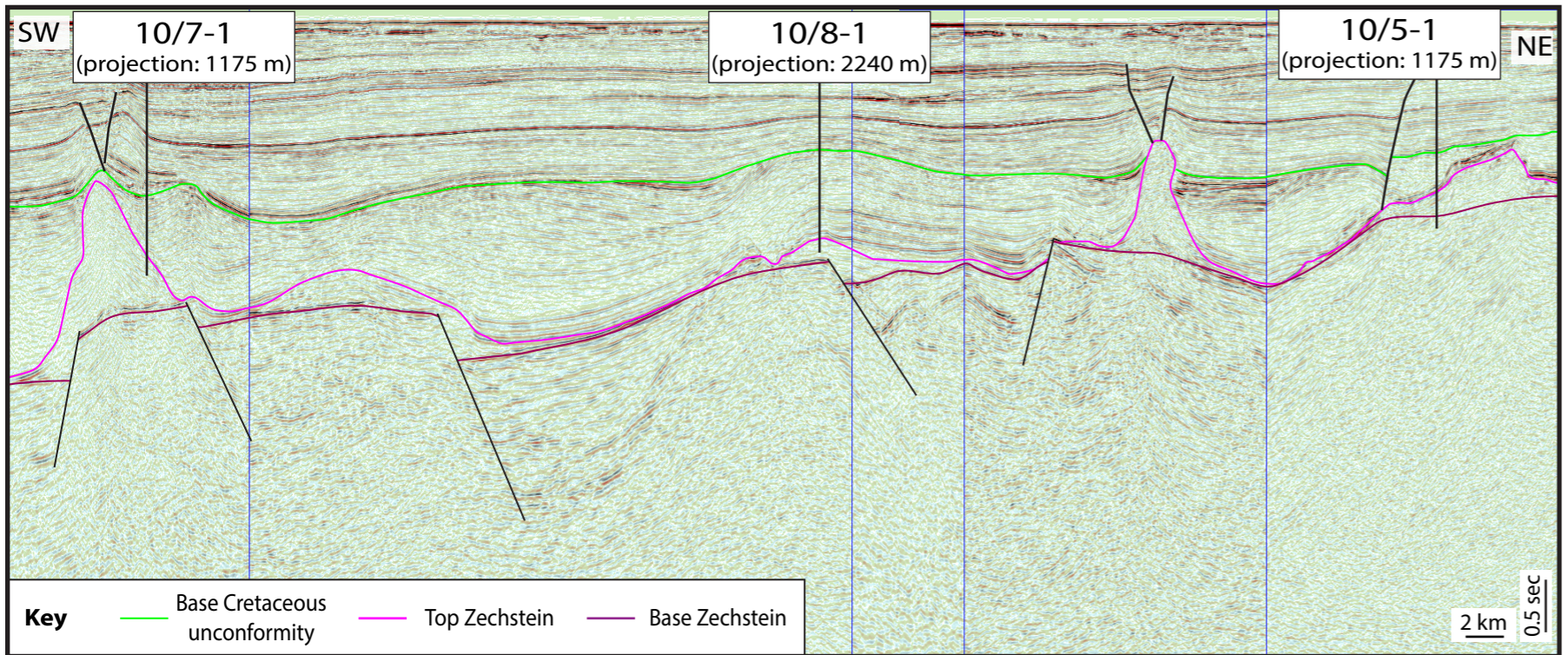
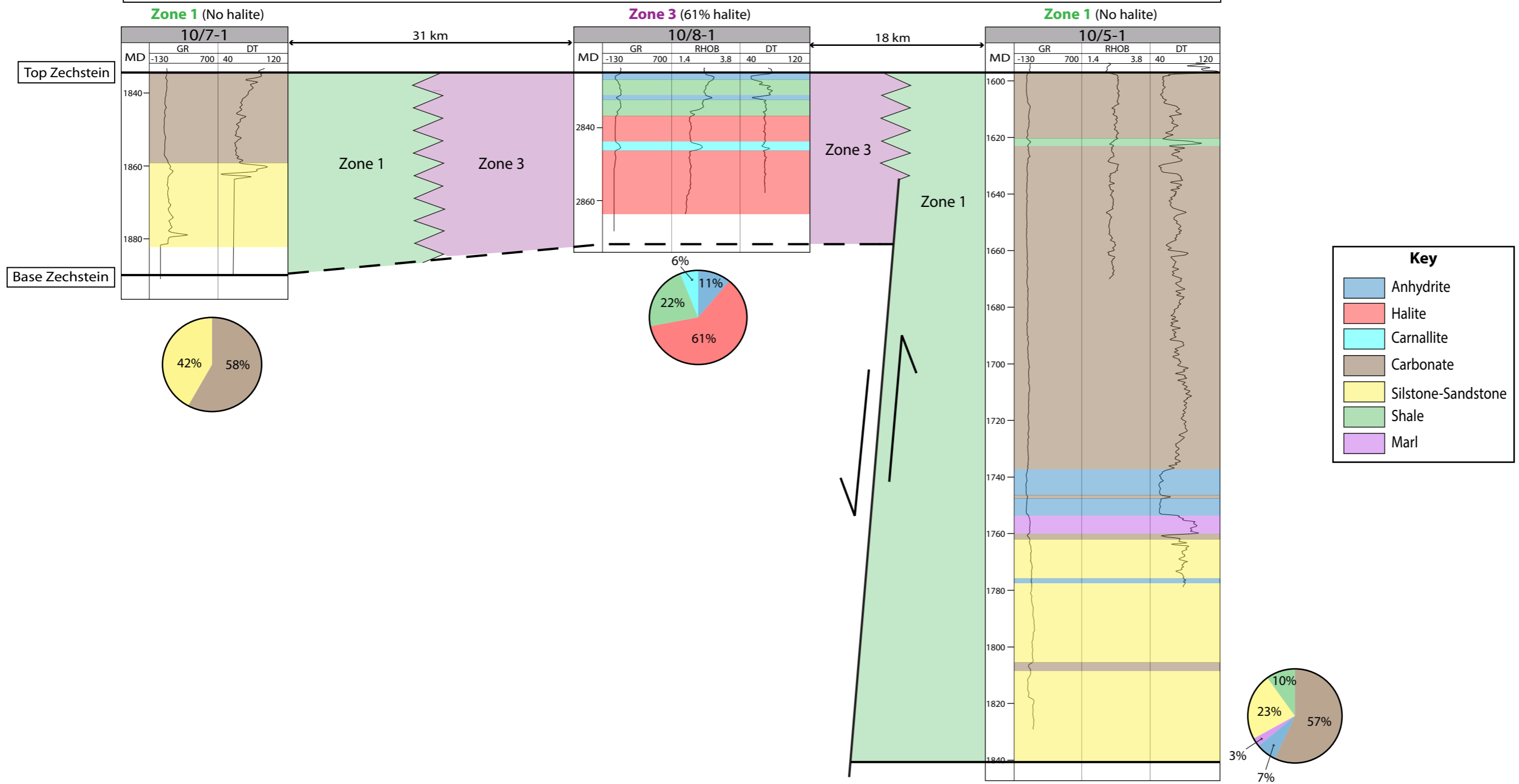


Figure 14

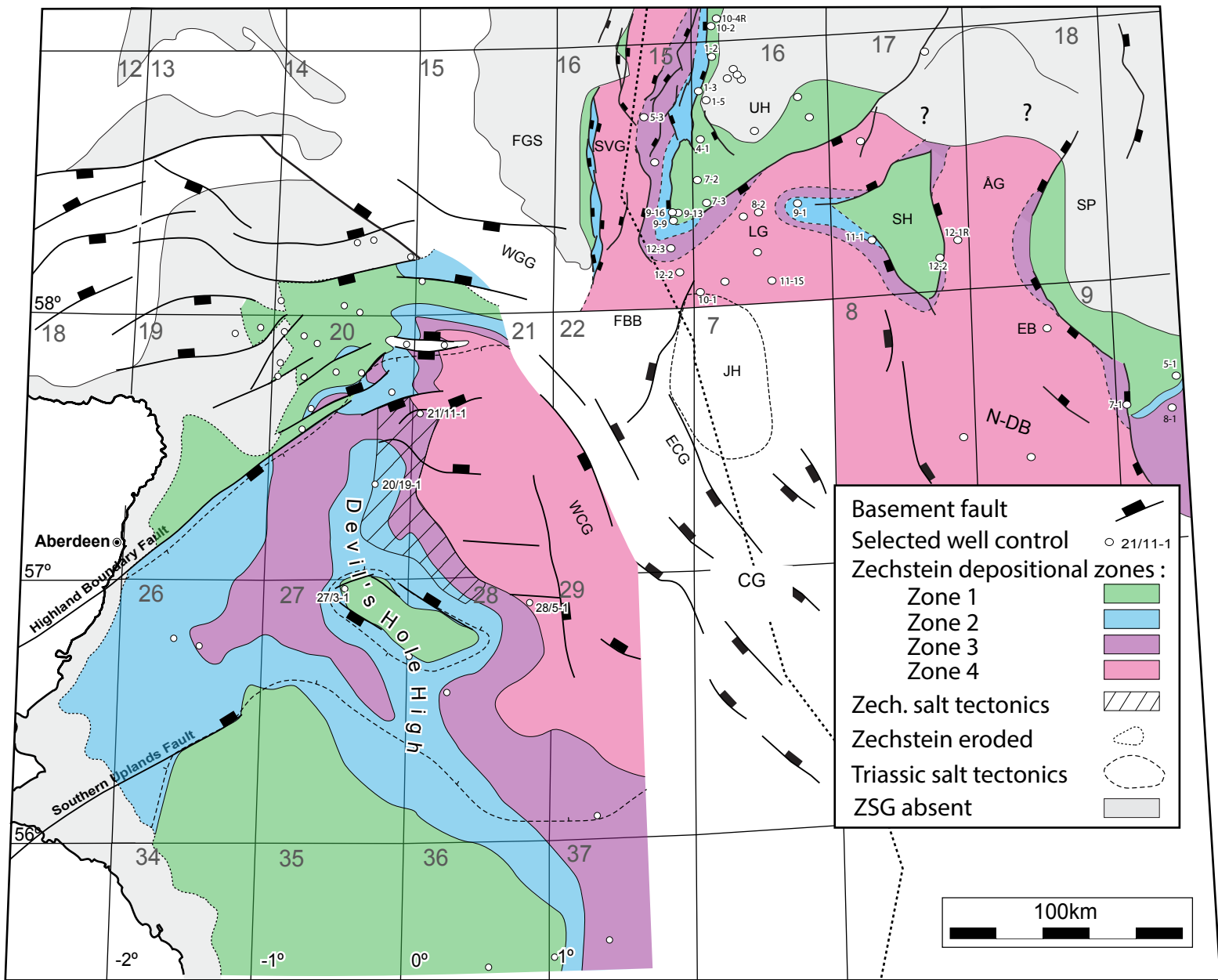
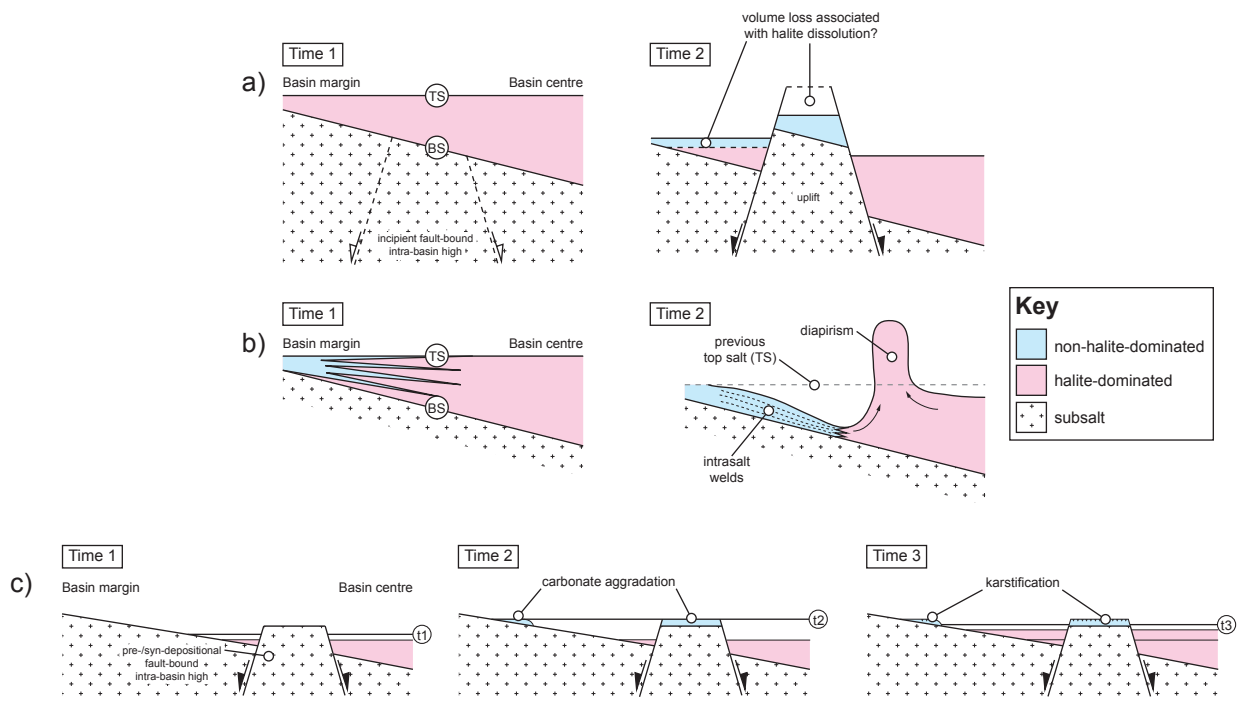


Figure 15

Fig. 16



Well name	Well-log data	TD (m)	ZSG Thickness (m)	Fully penetrate the ZSG?	Halite proportion	Inferred Depositional Zone (DZ)	Structural location	Comment
15/5-3	GR, RHOB, DT	5042	1046	Yes	93 %	4	South Viking Graben; deep basin	Penetrates off-centre of salt diapir
16/4-1	GR, RHOB, DT	2909	191	Yes	-	1	Utsira High; basin margin	Located 4 km SE of salt diapir
15/9-9	GR, RHOB, DT	3044	45	Yes	-	1	Sleipner Terrace; basin margin	
15/12-3	GR, RHOB, DT	4450	1203	Yes	71 %	3	Ling Graben; intra-basin terrace	Penetrates off-centre of salt diapir
15/12-2	GR, RHOB, DT	2924	37+	No	-	3?	Ling Graben; intra-basin terrace	Penetrates crest of salt diapir
15/9-16	GR, RHOB, DT	3120	55	Yes	-	1	Sleipner Terrace; basin margin	-
15/9-13	GR, RHOB	3280	25+	No	-	1?	Sleipner Terrace; basin margin	-
16/7-3	GR, RHOB, DT	3116	64	Yes	-	1	Sleipner Terrace; basin margin	-
16/8-2	GR, DT	3585	1325+	No	94 %	4	Ling Graben; deep basin	Penetrates off-centre of salt diapir
16/9-1	GR, DT	3340	140+	No	35 %	2?	Ling Graben; intra-basin terrace	-
25/10-4R	GR, RHOB, DT	2550	49+	No	-	1	Utsira High; basin margin	-
25/10-2R	GR, RHOB, DT	3153	126	Yes	-	1	Utsira High; basin margin	-
16/1-2	GR, RHOB, DT	2918	96	Yes	-	1	Utsira High; basin margin	-
16/7-2	GR, RHOB, DT	3146	107	Yes	-	1	Utsira High; basin margin	-
16/10-1	GR, RHOB, DT	3151	35+	No	66 %	3	Ling Graben; deep basin/intra-basin terrace	Penetrates off-centre of salt diapir crest
16/11-1S	GR, RHOB, DT	3050	794+	No	99 %	4	Ling Graben; deep basin/intra-basin terrace	Penetrates centre of salt diapir
17/11-1	GR, RHOB, DT	3270	755+	No	78 %	3	Ling Graben; intra-basin terrace	Penetrates off-centre of low-relief salt pillow
17/12-2	GR, RHOB, DT	2334	57	Yes	-	1	Sele High; basin margin	-
17/12-1R	GR, RHOB, DT	4298	165+	No	69 %	3	Egersund Basin; deep basin	Penetrates off-centre of low-relief salt pillow
10/7-1	GR, DT	1890	43	Yes	-	1	Lista Fault Block Complex; intra-basin terrace	-
10/8-1	GR, RHOB, DT	2861	36+	No	61 %	3	Lista Fault Block Complex; intra-basin terrace	Penetrates crest of salt pillow
10/5-1	GR, RHOB, DT	1842	245+	No	-	1	Lista Fault Block Complex; basin margin	Penetrates off-centre of salt diapir crest

Table 1

Lithology	Gamma-ray (API) (Schlumberger, 2009)	Density (RHOB, g/cm3) (Schlumberger, 2009)	Velocity (DT, US/F) (Schlumberger, 2009)
Anhydrite	0-70 (0-12)	2.4-3 (2.98)	45-90 (50)
Halite	0-30 (0)	2-2.3 (2.04)	65-75 (67)
Carbonate	40-160 (12-100)	2.5-2.8 (2.85)	45-80 (44)
Shale	35-650 (24-1000)	2-3 (2.65-2.7)	50-100 (60-170)
Carnallite	0-50 (220)	2-2.2 (1.57)	58-70 (N/A)

Table 2